Champneys, A. R., & Rodriguez-Luis, A. J. (1997). The non-transverse Shil'nikov-Hopf bifurcation ; uncoupling of homoclinic orbits and homoclinic tangencies.

Early version, also known as pre-print

The non-transverse Shil'nikov-Hopf bifurcation; uncoupling of homoclinic orbits and homoclinic tangencies

A.R. Champneys and A.J. Rodríguez-Luis
Dept. Engineering Mathematics Dept. Applied Mathematics
University of Bristol E.T.S.I.I., University of Sevilla
University Walk Camino de los Descubrimientos s/n
Bristol BS8 1TR 41092 Sevilla
U.K. Spain

Revised Version July 30, 1998

Abstract

It is known that in a neighbourhood of a codimension-two Shil'nikov-Hopf bifurcation, primary periodic orbits lie on a single wiggly curve in period–parameter space, with accumulation points at parameter values of a pair of homoclinic tangencies to a periodic orbit. In contrast, it has recently been shown by Hirschberg and Laing that primary periodic orbits lie on an infinity of isolas in a neighbourhood of certain degenerate homoclinic tangency to a periodic orbit. This paper analyses the codim 3 bifurcation caused by a non-transverse (that is, degenerately parametrically unfolded) Shil'nikov-Hopf bifurcation, which contains nearby dynamics akin to both degeneracies.

Two cases are classified as being downward pointing or upward pointing depending on whether the variation of a third parameter causes either the annihilation of a locus of saddle-focus homoclinic orbits to equilibria, or the uncoupling of this locus from the locus of Hopf bifurcations. We undertake a heuristic analysis of the unfolding, showing that in both cases it contains codimension-two non-transversal homoclinic orbits to equilibria and non-transversal homoclinic tangencies to periodic orbits. Unfolding the former non-transverse orbit, is shown to cause two wiggly curves to coalesce and leave finitely many isolas of periodic orbits. Unfolding the latter causes two wiggly curves to coalesce into first infinitely many and then finitely many isolas. Asymptotic expressions are given for the accumulation of two types of isola forming bifurcations. The implications of $\mathbb{Z}_2$-equivariance on the unfolding is discussed.

Finally, numerical evidence is presented for both upward and downward pointing non-transverse Shil'nikov-Hopf bifurcations occuring in a model of an autonomous nonlinear electronic circuit, both with respect to a $\mathbb{Z}_2$-equivariant and a $\mathbb{Z}_2$-non-equivariant equilibrium. Numerical computation of curves of periodic orbits, homoclinic orbits and homoclinic tangencies to periodic orbits are shown to agree broadly with the theory but to uncover extra complications.

1 Introduction

Homoclinic orbits to equilibria and homoclinic tangencies to periodic orbits are two codimension-one global bifurcations which represent organising centres in autonomous dynamical systems. Their analysis enables the understanding of complicated recurrent dynamics (see Wiggins (1990) and Guckenheimer & Holmes (1983) for summaries). In the former case, given certain conditions on the eigenvalues at the equilibrium Shil'nikov (1970) showed the existence of shift dynamics on a countably infinite number of symbols. Moreover, the bifurcation is accessible by following a single wiggly curve of periodic orbits undergoing a cascade of period-doubling and saddle-node bifurcations (Glendinning & Sparrow 1984). In the latter case, again a countably infinity of periodic orbits appear in a cascade of period-doubling and saddle-node bifurcations (Gavrilov & Shil'nikov (1972, 1973), Newhouse (1979)), but, in general, the periodic orbits lie on disconnected curves (Gaspard & Wang 1987) and the bifurcation is inaccessible by following a single periodic orbit.

A codimension-two bifurcation that links these two scenarios occurs when the equilibrium to which the orbit is homoclinic undergoes a super-critical Hopf bifurcation. An analysis of such a Shil'nikov-Hopf bifurcation dates back to Belyakov (1974), see also (Gaspard 1987, Hirschberg & Knobloch 1993, Bosch & Simó 1993, Lin 1993, Deng & Sakamoto 1995). For parameter-values just beyond the Hopf bifurcation, where a small amplitude periodic orbit exists, again a single wiggly curve of periodic orbits can be followed, this time accumulating on two parameter values corresponding to homoclinic tangencies to periodic orbits.

In contrast, Hirschberg & Laing (1995) have recently studied a two-parameter perturbation of a three-dimensional vector field containing a degenerate homoclinic tangency to a periodic orbit whose stable and unstable manifolds coincide. In the unfolding, one finds two curves in a parameter plane corresponding to non-degenerate (i.e. quadratic) homoclinic tangencies. The infinity of periodic orbits close to these tangencies are then shown to lie on isolas in a one-parameter bifurcation diagram with the left and right limit points on each isola converging on the parameter values of the two homoclinic tangencies.

This paper shall address how these two conflicting codimension-two scenarios may be linked by a single codimension-three degeneracy. Specifically we shall consider the case when a curve of homoclinic orbits intersects a Hopf-bifurcation curve non-transversally. In a neighbourhood of such a degeneracy one should expect to find curves in three-parameter space of Shil'nikov-Hopf bifurcations and non-transverse homoclinic tangencies. Note, however, that such a non-transverse homoclinic tangencies would be due to bad parameter variation rather than a degeneracy in the intersections of the stable and unstable manifolds of the periodic orbit, as in the case studied by Hirschberg and Laing. The key question is the mechanism by which a single wiggly-curve of periodic orbits may break up into infinitely many isolas. Our approach will be to conduct an analysis of an unfolding of the codim 3 singularity, and then to illustrate the results by numerical computations on a system modelling an electronic oscillator (Freire, Rodríguez-Luis, Gamero & Ponce 1993). In fact, the dynamics of this example system are additionally complex, and there is evidence that infinitely many codimension-three non-transverse Shil'nikov-Hopf bifurcations occur (Fernández-Sánchez, Freire & Rodríguez-Luis 1997*a*, Fernández-Sánchez, Freire, Gamero & Rodríguez-Luis 1997).

For simplicity we study only three-dimensional vector fields, which we assume to exhibit the codimension-three global bifurcation. Using 'homoclinic center-manifold' results as in Sandstede (1993), it should be possible to adapt our results to systems of arbitrary dimension greater than three, which posses the same degeneracy. Also, we do not attempt to be completely rigorous. Instead we concentrate

on the analysis of approximate Poincaré maps, closely following the approach of Hirschberg & Knobloch (1993). For an indication of how to pose rigorous results, the reader is referred to Belyakov (1974), Lin (1993) and Deng & Sakamoto (1995) which treat the codim 2 non-degenerate Shil'nikov-Hopf bifurcation. We also mention related analysis by Gaspard (1987) and Bosch & Simó (1993).

The rest of the paper is outlined as follows. In Section 2, we construct Poincaré maps describing the unfolding of the non-transverse Shil'nikov-Hopf bifurcation and analyse the behaviour of primary global bifurcations. Section 3 considers periodic orbits obtained by fixed points of these maps, and analyses transformations of their one-parameter bifurcation diagrams as two unfolding parameters are varied. We also look briefly at the influence of an odd symmetry. Section 4 presents the numerical example, and finally, Section 5 contains some conclusions and suggestions for future work.

2 The codimension-three degeneracy and its unfolding

Consider a three-parameter family of vector fields of the form

$$\begin{pmatrix} \dot{x} \\ \dot{y} \\ \dot{z} \end{pmatrix} = \begin{bmatrix} \mu & -\omega & 0 \\ \omega & \mu & 0 \\ 0 & 0 & \lambda \end{bmatrix} \begin{pmatrix} x \\ y \\ z \end{pmatrix} + \begin{pmatrix} Q(x,y,z;\mu,\nu,\sigma) \\ R(x,y,z;\mu,\nu,\sigma) \\ S(x,y,z;\mu,\nu,\sigma) \end{pmatrix}, \tag{2.1}$$

where $\lambda > 0$, $\omega \neq 0$, Q, R and S are nonlinear functions that vanish together with their first derivatives at $(x,y,z) = (0,0,0)$, and there are no degeneracies other than those described as follows (see Figs. 1 and 2). Suppose that when $\mu = 0$, a non-degenerate supercritical Hopf bifurcation occurs with a stable limit cycle C existing for $\mu > 0$. Furthermore, for a 2-parameter manifold of parameter values passing through $(\mu,\nu,\sigma) = (0,0,0)$, the branch $W^{uu}_+(0)$ of the strongly unstable manifold of the origin that is tangent as $t \to -\infty$ to the positive z-axis returns under the flow to become asymptotic to $W^s(0)$ as $t \to +\infty$. Here, for simplicity, we continue to label the two-dimensional invariant manifold that is tangent to $\{z = 0\}$ at 0 as $W^s(0)$ even for $\mu \geq 0$ when the origin ceases to be a saddle. For $\mu < 0$ the orbit in question, Γ, corresponds to a homoclinic orbit to the origin, whereas for $\mu > 0$ it corresponds to a large heteroclinic connection between the origin and the periodic orbit C born in the Hopf bifurcation. Here we differentiate between a *small* 0-to-C heteroclinic orbit that is contained in $W^s(0)$ and which exists for all $\mu > 0$, and a *large* heteroclinic orbit formed by $W^{uu}_+(0)$. Suppose that the lower branch $W^{uu}_-(0)$ of the strong unstable manifold never returns to a neighbourhood of the origin for sufficiently small μ, σ, ν.

In contrast to previous studies, we assume that the situation is further degenerate in that, when $\mu = \nu = 0$, the intersection of $W^{uu}_+(0)$ and $W^s(0)$ is non-transversal as σ varies. Specifically, we assume that, in the extended phase space obtained by appending $\dot{\sigma} = 0$ to (2.1), the two manifolds have a simple quadratic tangency. We suppose that ν unfolds this tangency in a generic way. For definiteness, when $\sigma = \mu = 0$, $W^{uu}_+(0)$ returns above $W^s(0)$ for $\nu > 0$ and below $W^s(0)$ for $\nu < 0$. With reference to Figs. 1 and 2, we note that such an unfolding can occur in two ways. We refer to the two cases as upward or downward pointing depending on whether, at $\nu = 0$, the quadratic curve of parameter values of homoclinic (or large heteroclinic) orbits points into the region where the origin is completely unstable ($\mu > 0$) or into the region where the origin is a saddle-focus ($\mu < 0$). Also depicted in Figs. 1 and 2 are parameter sheets of homoclinic tangencies to C. The shape of these curves is calculated in Section 2.2 below.

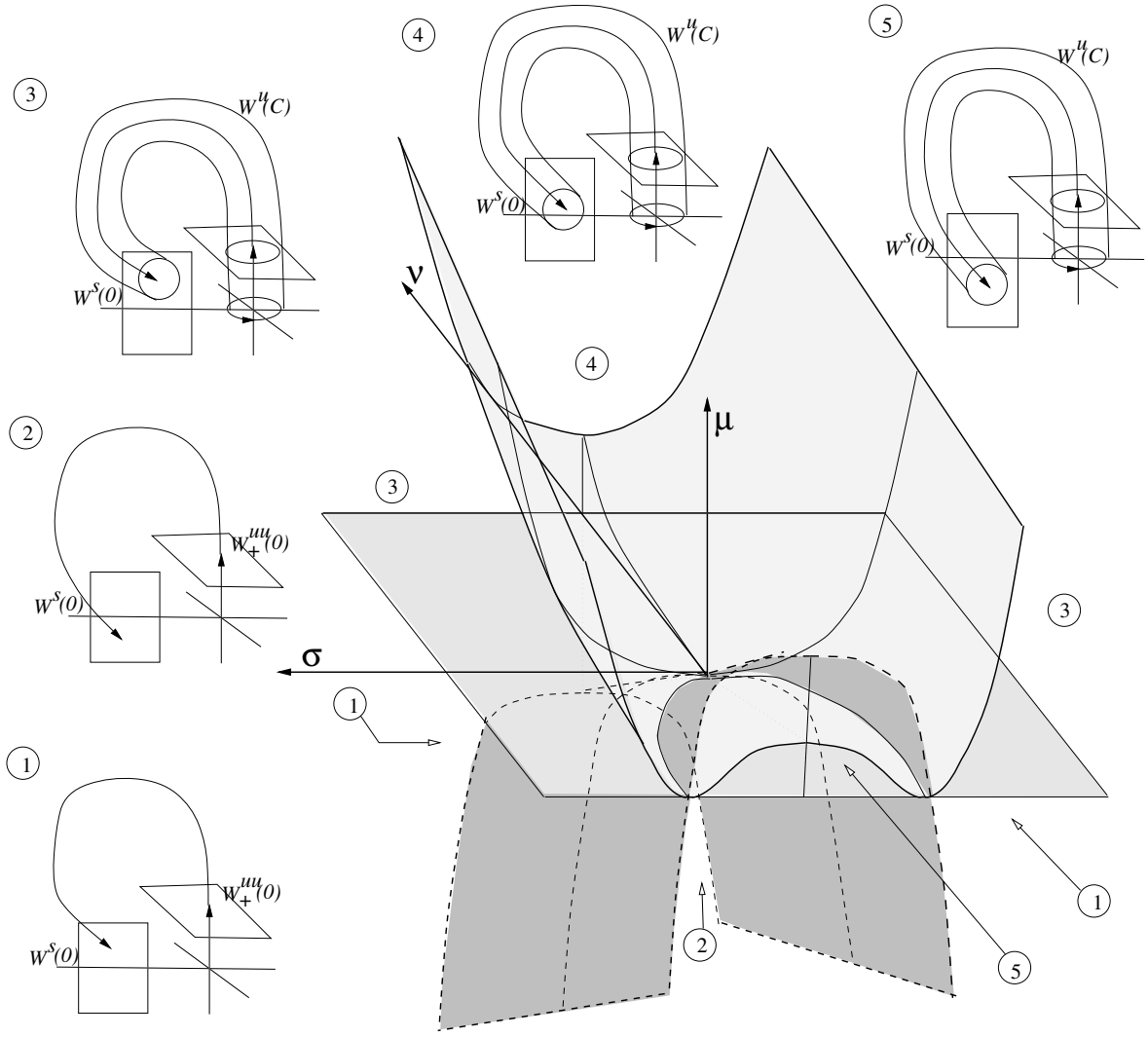

Figure 1: Depicting global bifurcation surfaces and associated phase portraits of (1) in the upward-pointing case. The surface bounded by dashed lines corresponds to parameter values of homoclinic orbits to the origin ($\mu < 0$) or large heteroclinic orbits from 0 to C ($\mu > 0$). The surface bounded by solid lines correspond to homoclinic tangencies to C, and the horizontal section ($\mu = 0$) is the Hopf-bifurcation manifold. Typical cross-sections through the surfaces are shown in Fig. 4 below.

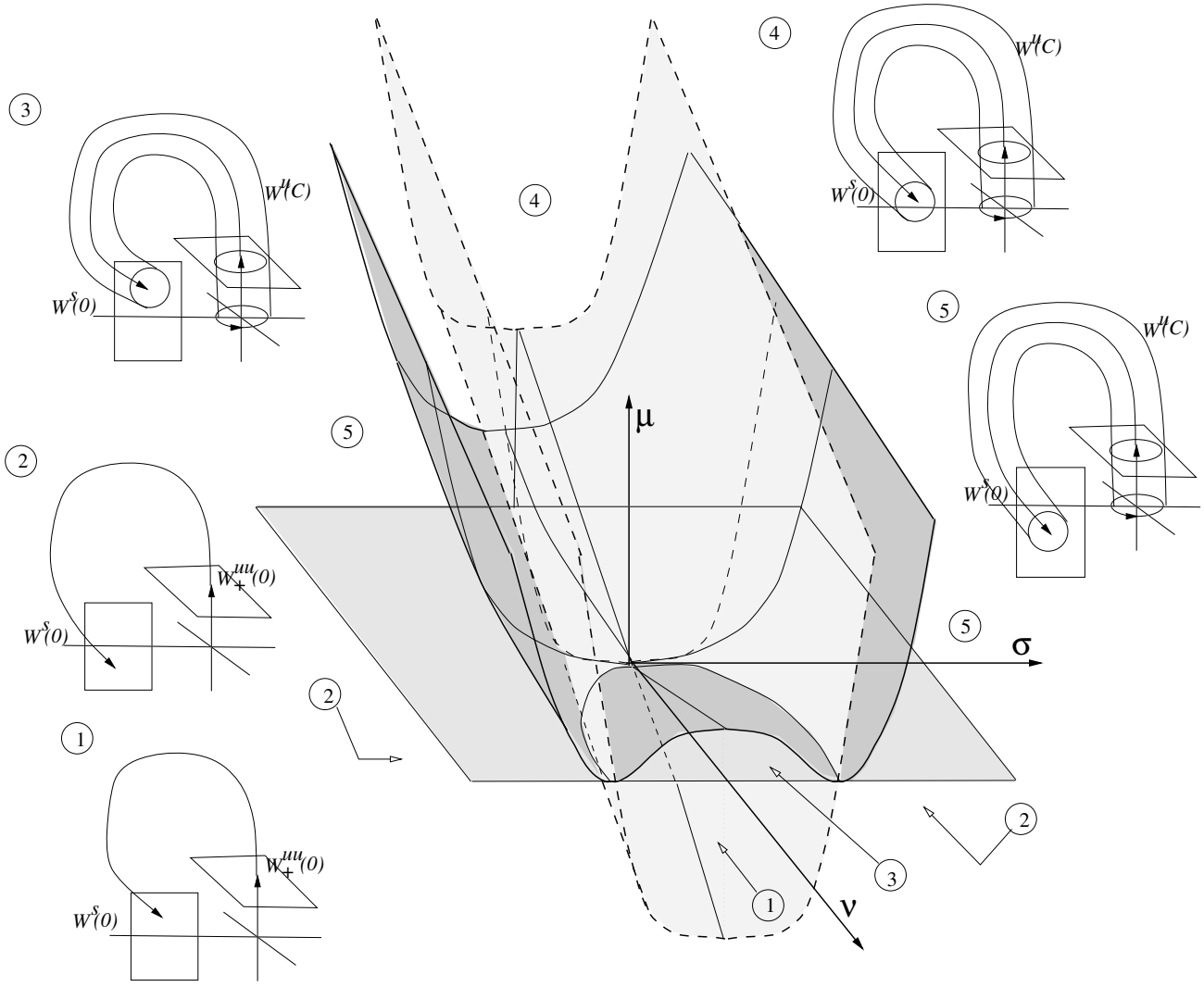

Figure 2: The analogue of Fig. 1 for the downward-pointing case. Typical cross-sections are given in Fig. 5. below.

2.1 Construction of Poincaré maps

Following Hirschberg & Knobloch (1993), we construct an approximation to the flow of (2.1) in a neighbourhood of Γ. See Fig. 3. Consider two Poincaré sections Σ_0 and Σ_1 given by

$$\begin{aligned} \Sigma_0 &: \{(x,y,z) \mid y = 0, \zeta < x \leq \varepsilon\}, \\ \Sigma_1 &: \{(x,y,z) \mid z = \varepsilon\}. \end{aligned}$$

An approximate local Poincaré map from Σ_0 to Σ_1 is constructed by assuming that the dynamics inside the box $\{x \leq \varepsilon, y \leq \varepsilon, 0 < z \leq \varepsilon\}$ are governed by the truncated equations (in polar co-ordinates with $x = r\cos\theta$, $y = r\sin\theta$)

$$\begin{aligned} \dot{r} &= r(\mu - r^2), \\ \dot{\theta} &= \omega, \\ \dot{z} &= \lambda z. \end{aligned} \tag{2.2}$$

Note that the periodic orbit, which exists for $\mu > 0$ is thus $C := \{r = \sqrt{\mu}, z = 0\}$ in these local co-ordinates. The local Poincaré map is given by

$$\begin{aligned} T_0 : (x_0, z_0) &\mapsto (x_1, y_1) \\ x_1 &= R(x_0, \tau(z_0), \mu)\cos[(\omega/\lambda)\ln(\varepsilon/z_0)], \\ y_1 &= R(x_0, \tau(z_0), \mu)\sin[(\omega/\lambda)\ln(\varepsilon/z_0)] \end{aligned} \tag{2.3}$$

where

$$R(x_0, \tau(z_0), \mu) = \begin{cases} x_0 e^{\mu\tau}\{1 + 2\tau x_0^2[\sinh(\mu\tau)/(\mu\tau)]e^{\mu\tau}\}^{-1/2}, & \mu \neq 0 \\ x_0(1 + 2x_0^2\tau)^{-1/2}, & \mu = 0 \end{cases}$$

and

$$\tau(z_0) = (1/\lambda)\ln(\varepsilon/z_0).$$

$\tau(z_0)$ is the time of flight from Σ_0 to Σ_1.

In order to construct a global Poincaré map T_1 from Σ_1 to Σ_0, an assumption needs to be made about the first intersection of W_+^{uu} with Σ_1 as parameters vary. In keeping with the supposed behaviour in the unfolding of the degeneracy we assume that this point of intersection is given by

$$x = \overline{x} = \overline{x_0} + a\mu + b\nu + c\sigma, \tag{2.4}$$

$$z = \overline{z} = \nu + d\mu + (e\nu + f\mu)\sigma \pm \sigma^2, \tag{2.5}$$

where $\overline{x_0}$, a, b, c, d, e and f are unknown coefficients with $\zeta < \overline{x_0} < \varepsilon$. Note that one is free to choose the parameters ν and σ so that the coefficient of ν in (2.5) is unity and the coefficient of σ^2 is ± 1. Also, for definiteness we shall henceforth assume that $d > 0$. Then, the sign '+' corresponds to the upward pointing case and the sign '–' corresponds to the downward pointing case. The case with $d < 0$ can be analysed similarly and leads to no qualitative differences, the important quantity being the sign of $d\nu$.

The map T_1 is then approximated by its constant and linear terms:

$$T_1 : (x_1, y_1) \mapsto (x, z)$$

$$\begin{pmatrix} x \\ z \end{pmatrix} = \begin{bmatrix} \alpha & \gamma \\ \kappa & \beta \end{bmatrix} \begin{pmatrix} x_1 \\ y_1 \end{pmatrix} + \begin{pmatrix} \overline{x} \\ \overline{z} \end{pmatrix}, \tag{2.6}$$

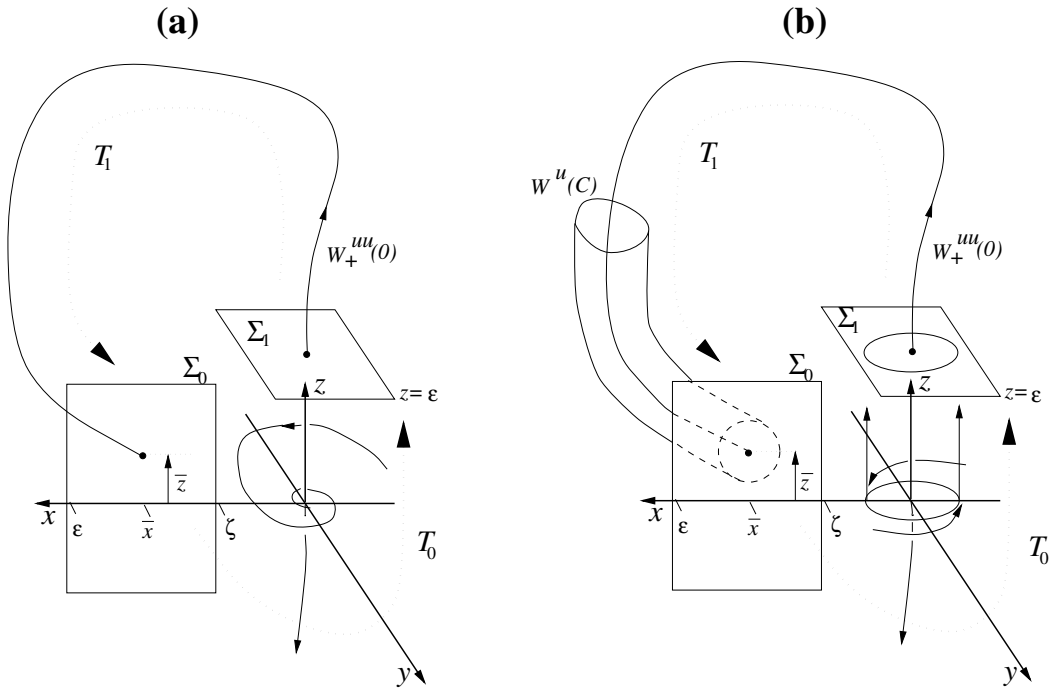

Figure 3: The Poincaré maps approximating the flow of (2.1); **(a)** for $\mu < 0$, **(b)** for $\mu > 0$.

where $\overline{x}$ and $\overline{z}$ are given by (2.4), (2.5) and α, β, γ and κ are unknown coefficients satisfying the non-degeneracy condition $\alpha\beta - \gamma\kappa \neq 0$. Finally, we suppose that ε and ζ are chosen appropriately in order to make T_1 uniquely defined (see Hirschberg & Knobloch (1993)[Sect. 5]).

The first return map $T = T_1 \circ T_0 : \Sigma_0 \to \Sigma_0$ is now obtained from (2.3) and (2.6), giving

$$T : \begin{pmatrix} x \\ z \end{pmatrix} = F(x_0, z_0, \mu) \begin{pmatrix} A\cos[(\omega/\lambda)\ln(z_0/\varepsilon) - \Phi_1)] \\ B\cos[(\omega/\lambda)\ln(z_0/\varepsilon) - \Phi_2)] \end{pmatrix} + \begin{pmatrix} \overline{x} \\ \overline{z} \end{pmatrix}, \tag{2.7}$$

where

$$\begin{aligned} A\cos(\Phi_1) &= \alpha, \qquad B\cos(\Phi_2) = \kappa, \\ A\sin(\Phi_1) &= \gamma, \qquad B\sin(\Phi_2) = \beta \end{aligned}$$

and

$$F(x_0, z_0, \mu) = \begin{cases} x_0 v_0^{-\delta} \left\{1 + (x_0^2/\mu)(v_0^{-\delta} - v_0^{\delta})v_0^{-\delta})\right\}^{-1/2}, & \mu \neq 0 \\ x_0 \left\{1 - (2x_0^2/\lambda)\ln(v_0)\right\}^{-1/2}, & \mu = 0 \end{cases}$$

with

$$\delta = \mu/\lambda \quad \text{and} \quad v_0 = z_0/\varepsilon.$$

Apart from the expressions (2.4) and (2.5) for $\overline{x}$ and $\overline{z}$, (2.7) is identical to the map derived by Hirschberg & Knobloch (1993)[Sect. 2] in the neighbourhood of a non-degenerate Shil'nikov-Hopf bifurcation. The parameter $|\delta|$ is the critical parameter appearing in the analysis of Shil'nikov homoclinic orbits (Glendinning & Sparrow 1984) with the critical condition for the existence of shift dynamics being $0 < -\delta < 1$ at the parameter values for which a homoclinic orbit exists[1]. Moreover, there is a

[1]In the Russian Literature, the critical parameter is often taken to be the so called 'saddle quantity' $s = \mu + \lambda$, with the condition for shift dynamics being $s > 0$.

distinction in the dynamics, notably in the stability of periodic orbits, depending on the sign of $|\delta| - 1/2$. Since $\delta \to 0$ at a Shil'nikov-Hopf point, we shall assume throughout that μ is sufficiently small and certainly small enough to make $|\delta| < 1/2$. Then the envelope function F satisfies

$$\lim_{z\to 0} F(x,z,\mu) = \begin{cases} 0, & \mu \le 0 \\ \sqrt{\mu}, & \mu > 0 \end{cases}, \quad \lim_{z\to 0} \frac{\partial F(x,z,\mu)}{\partial z} = \infty, \quad \lim_{z\to 0} \frac{\partial^2 F(x,z,\mu)}{\partial z^2} < 0.$$

Note that taking $\sigma = 0$ and allowing (μ, ν) to be unfolding parameters, results in a non-degenerate Shil'nikov-Hopf bifurcation, duplicating the results of Belyakov (1974), Hirschberg & Knobloch (1993), etc. Here we are interested in the degenerate bifurcation that occurs with $\nu = 0$ and (μ, σ) as parameters. We then regard ν as a parameter which unfolds this degenerate situation.

2.2 Primary global bifurcations

2.2.1 Upward pointing case

We consider first the upward pointing case. By construction, parameter regions corresponding to homoclinic orbits to 0 or large 0-to-C heteroclinic orbits are given by $\overline{z} = 0$, which implies

$$\nu + d\mu + (e\nu + f\mu)\sigma + \sigma^2 = 0. \tag{2.8}$$

When $e = f = 0$, (2.8) for fixed ν, is the equation of a parabola in the (μ, σ)-plane, intersecting the μ-axis at $\mu = -\nu/d$. If $\nu < 0$, the parabola intersects the σ-axis twice, which gives two Shil'nikov-Hopf bifurcation points. For non-zero e and f, (2.8) is the equation of a hyperbola. One branch of the hyperbola also intersects the μ-axis at $\mu = -\nu/d$ and, for $\nu < 0$, intersects the σ-axis twice for small ν. The σ-values of these Shil'nikov-Hopf bifurcation points are given by

$$\sigma^u_{h\pm} \;=\; -(1/2)(e\nu \mp \sqrt{e^2\nu^2 - 4\nu}) \;=\; \pm\sqrt{-\nu} + \mathcal{O}(\nu). \tag{2.9}$$

The other branch of the hyperbola does not intersect the region where σ and ν are both small and so will not concern us in what follows.

We next locate the curve corresponding to a tangency between the stable and unstable manifolds of C for $\mu > 0$. Such a curve exists when the tubular manifold depicted in Fig. 3(b) returns to Σ_0 tangent to $\{(x, y, z) \mid z = 0\}$. The co-ordinates of $W^u(C) \cap \Sigma_0$ may be parametrised by $0 \le s < 2\pi$ as in Hirschberg & Knobloch (1993)

$$x(s) = A\sqrt{\mu}\cos(s - \Phi_1) + \overline{x}, \quad z(s) = B\sqrt{\mu}\cos(s - \Phi_2) + \overline{z}. \tag{2.10}$$

From (2.10) it is easy to see that the required tangency occurs when $\pm B\sqrt{\mu} = \overline{z}$, which implies

$$B^2\mu = \{\nu + d\mu + (e\nu + f\mu)\sigma + \sigma^2\}^2. \tag{2.11}$$

For fixed ν sufficiently small, the relation (2.11) can be expressed in the form of μ as a function of σ, for small σ. Plots of the curves (2.8) and (2.11) are presented in Fig. 4 for three values of ν and certain fixed values of the other constant coefficients. The qualitative shape of the curve (2.11) is, for small (μ, σ), as depicted in Fig. 4. In particular, when $\nu < 0$, there are three turning points of μ with respect to σ, for small μ given by $(\sigma, \mu) = (\sigma^u_{h\pm}, 0)$, (σ^u_t, μ^u_t), where $\sigma^u_{h\pm}$ are the σ-values of the two Shil'nikov-Hopf points given by (2.9), and

$$\sigma^u_t = -(1/2)e\nu - (f/2B^2)\nu^2 + \mathcal{O}(\nu^3), \quad \mu^u_t = \nu^2/B^2 + \mathcal{O}(\nu^3). \tag{2.12}$$

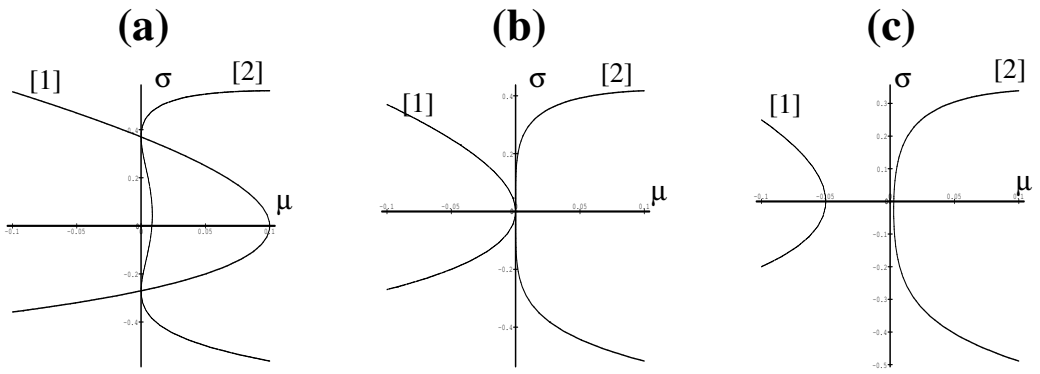

Figure 4: Upward-pointing case: Curves [1] of homoclinic orbits to 0 and large 0-to-C heteroclinic orbits given by (2.8) and [2] of homoclinic tangencies to C given by (2.11) for $B = d = e = f = 1$ and **(a)** $\nu = -0.1$, **(b)** $\nu = 0$ and **(c)** $\nu = 0.05$.

When $\nu = 0$, all three turning points combine at $\sigma = \mu = 0$ and the graph of $\mu(\sigma)$ is locally quartic rather than quadratic. For $\nu > 0$, there is a unique turning point given by (2.12), which occurs for $\mu > 0$, and all other points on the curve for small σ satisfy $\mu > \mu_t^u$. Hence there are no homoclinic tangencies locally for $0 < \mu < \mu_t^u(\nu)$ for $\nu > 0$. We conclude that the unfolding of primary homoclinic orbits and tangencies in this case is as depicted in Fig. 1.

2.2.2 Downward pointing case

Curves of primary connections between $W_+^{uu}(0)$ and $W^s(0)$ are now given by

$$\nu + d\mu + (e\nu + f\mu)\sigma - \sigma^2 = 0 \tag{2.13}$$

which intersects the μ-axis at $\mu = -\nu/d$ and, for $\nu > 0$, intersects the σ-axis at

$$\sigma = \sigma_{h\pm}^d \;=\; (1/2)(e\nu \pm \sqrt{e^2\nu^2 + 4\nu}) \;=\; \pm\sqrt{\nu} + \mathcal{O}(\nu). \tag{2.14}$$

Hence there are two Shil'nikov-Hopf points for $\nu > 0$ and none for $\nu < 0$. For $\nu < 0$ the branch of the hyperbola (2.13) is contained completely in the right-half plane and hence there are no longer any homoclinic orbits to the origin locally. Instead, the curve corresponds exclusively to 0-to-C heteroclinic connections (see Fig. 5).

Using (2.10), homoclinic tangencies to C are now given by

$$B^2\mu = \{\nu + d\mu + (e\nu + f\mu)\sigma - \sigma^2\}^2. \tag{2.15}$$

As was the case for (2.11), for fixed ν, solutions to (2.15) can be expressed as a graph of μ against σ for small (σ, ν). This curve is qualitatively as depicted in Fig. 5, which shows the analogue of Fig. 4 for the downward pointing case. In particular, note that the non-transverse homoclinic tangency now occurs at

$$\sigma_t^d = (1/2)e\nu(f/2B^2)\nu^2 + \mathcal{O}(\nu^3), \quad \mu_t^d = \nu^2/B^2 + \mathcal{O}(\nu^3). \tag{2.16}$$

Hence the unfolding of primary homoclinic orbits and tangencies is as depicted in Fig. 2.

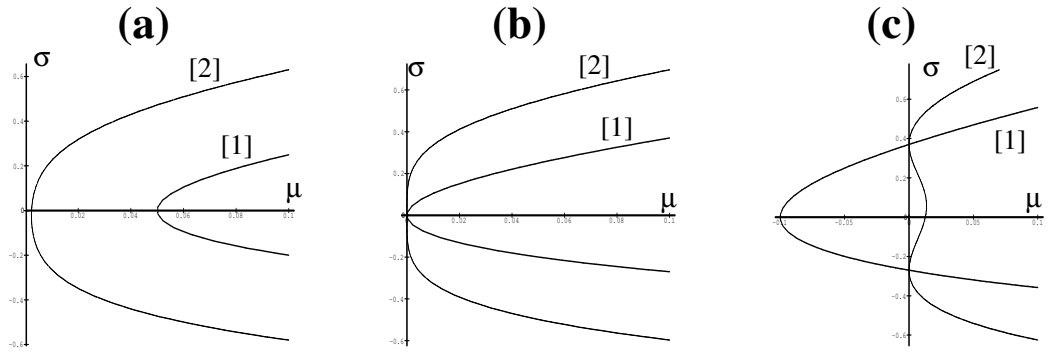

Figure 5: The analogue of Fig. 4 for the downward-pointing case. Curves [1] of homoclinic and heteroclinic orbits given by (2.13) and [2] of homoclinic tangencies to C given by (2.15) for $B = d = e = f = 1$ and **(a)** $\nu = -0.1$, **(b)** $\nu = 0$ and **(c)** $\nu = 0.1$.

3 Periodic Orbits

Primary periodic orbits, that is, orbits which make one passage through a tubular neighbourhood surrounding Γ, are given by fixed points of the map (2.7). Upon imposing such a condition for fixed points, note that $x = \overline{x} + \mathcal{O}(\sqrt{\mu}, \sigma, \nu)$. Hence for small μ, σ and ν one can approximately uncouple the equation for z to obtain

$$z - \overline{z} = BF(\overline{x}, z, \mu)\cos[(\omega/\lambda)\ln(z/\varepsilon) - \Phi_2)] \tag{3.1}$$

to leading order. Following Glendinning & Sparrow (1984), fixed points of (3.1) are determined graphically by plotting both sides of the equation as a function of z as a single parameter is varied. The results can then be plotted as period against parameter, upon noting from (2.3) that

$$\text{Period} \approx \text{const.} + (1/\lambda)\ln(\varepsilon/z).$$

We choose to fix ν and μ and allow σ to vary. We shall treat the upward and downward pointing cases separately.

3.1 Upward pointing case

The left-hand side of (3.1) is

$$z - (\nu + d\mu + (e\nu + f\mu)\sigma + \sigma^2).$$

We consider separately bifurcation sequences of primary periodic orbits on either side of the Hopf bifurcation, that is, $\mu > 0$ or $\mu < 0$.

3.1.1 Saddle-focus region

Consider first $\mu = \mu_1 < 0$. Here the dynamics are qualitatively different depending on the sign of $\nu - \nu_a(\mu_1)$, where $\nu_a(\mu_1) > 0$ is the ν-value at which the apex of the locally quadratic curve in (σ, ν)-space $\overline{z} = 0$ given by (2.8) occurs at $\mu = \mu_1$ (see Fig. 4(c)). The results of the graphical analysis

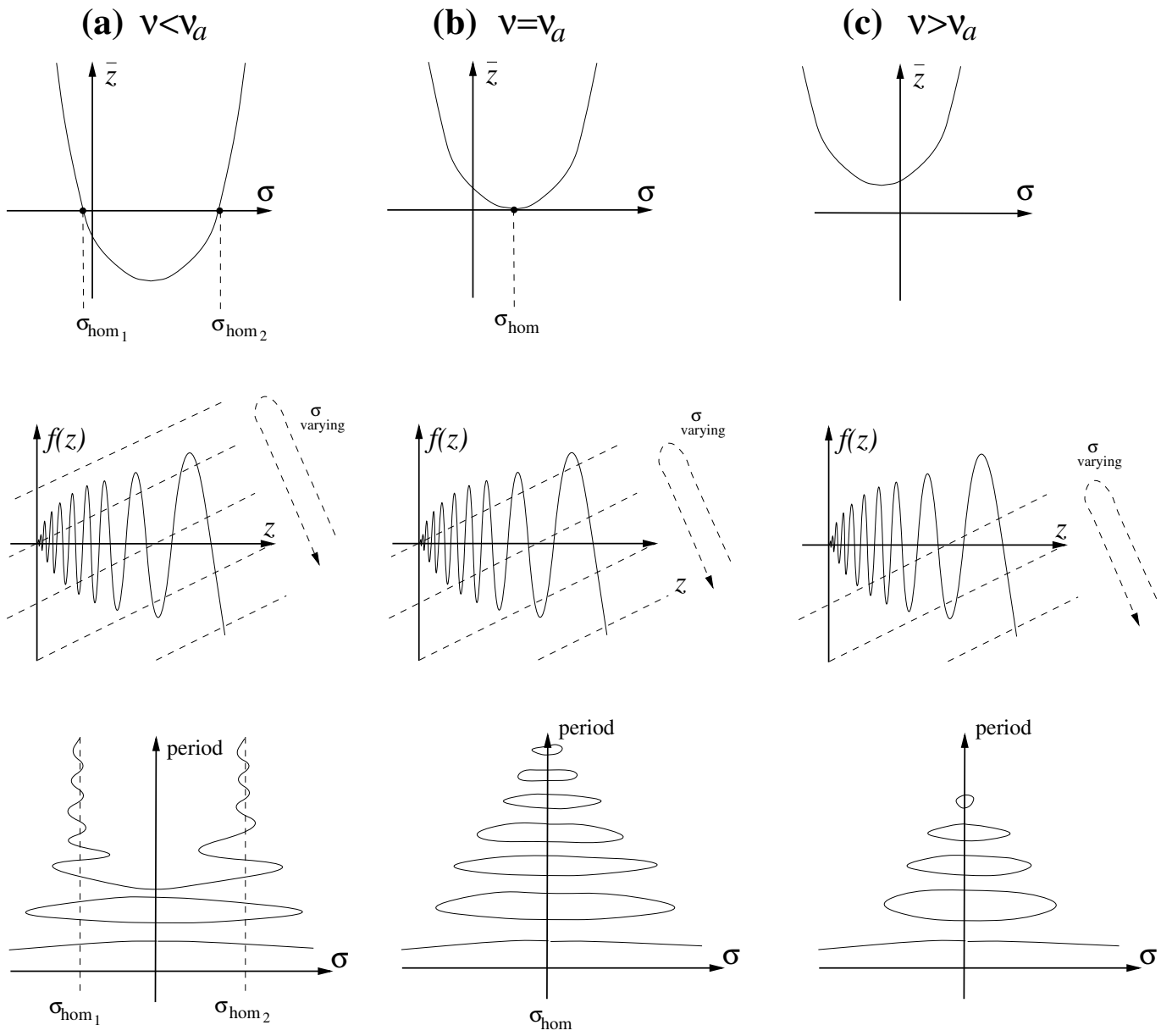

Figure 6: Periodic orbits in the vicinity of Shil'nikov homoclinic orbits for fixed $\mu_1 < 0$ and three indicative values of ν. In each case, the top sketch depicts $\overline{z}$ as a function of σ, the middle sketch depicts intersections between the left-hand and right-hand sides of (3.1) and the bottom sketch shows bifurcation diagrams of periodic orbits.

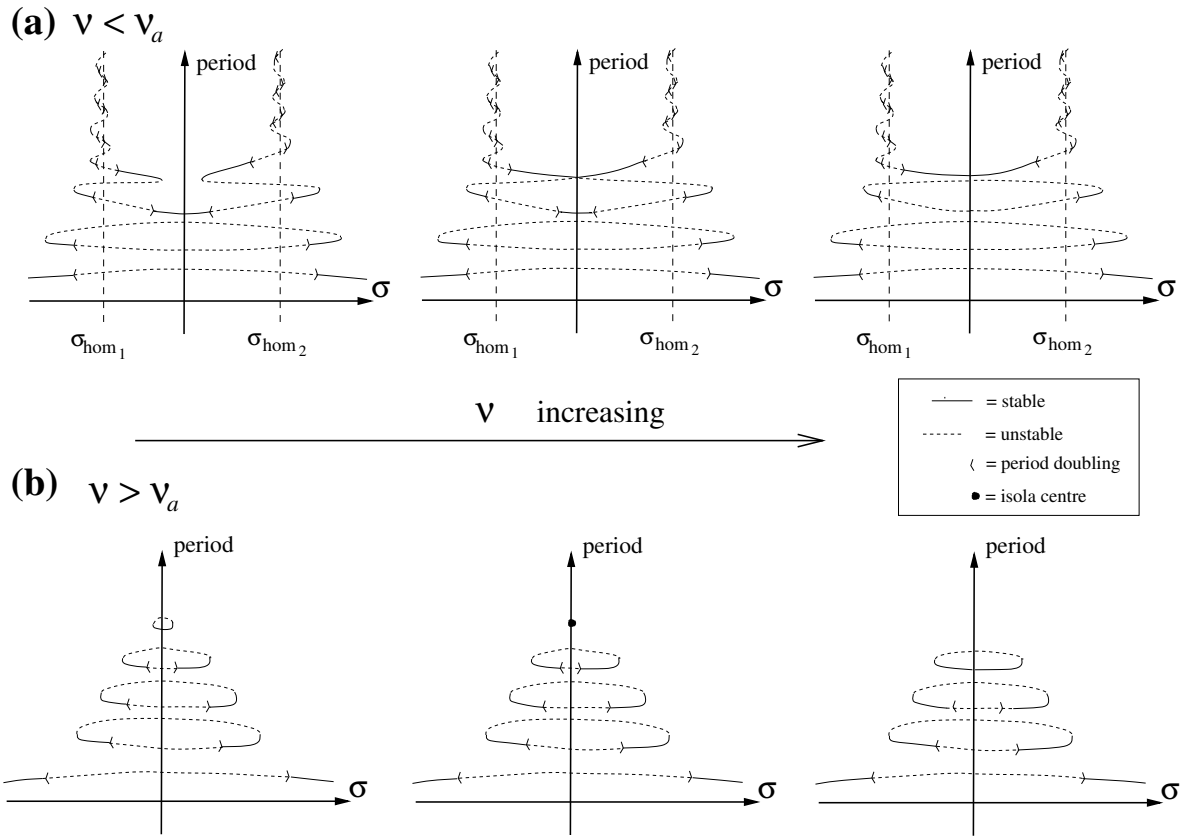

Figure 7: Showing the mechanism of isola formation and destruction as ν varies in σ versus period bifurcation diagrams of primary periodic orbits. Conjectures on the stability of the periodic orbits (for the time-reversed system) are also given.

are shown in Fig. 6. It is clear from the figure that the destruction of Shil'nikov homoclinic orbits, at $\nu = \nu_a$, causes the existence of isolas of periodic orbits. An infinite number exist for $\nu = \nu_a$, whereas only a finite number exist for $\nu \neq \nu_a$.

For $\nu < \nu_a$, where two distinct primary homoclinic orbits exist, there are two wiggly curves in the period-versus parameter plot, which representing primary periodic orbits approaching each homoclinic orbit as described by Glendinning & Sparrow (1984). As ν increases, isolas are successively created by collision of two adjacent limbs of the wiggly curves, in codim 2 transcritical bifurcations. See Fig. 7(a). Similar transcritical bifurcations were observed in the example system studied in Champneys (1991). There, such bifurcations were termed homoclinic switching bifurcations because, as ν increases, a switch occurs between which low-amplitude periodic orbit forms a continuous branch (the wiggly curve) approaching homoclinicity.

For $\nu > \nu_a$ the only primary periodic orbits for small σ are those on the finitely-many surviving isolas, which, for fixed $\nu > \nu_a$, have a strict upper bound on their period. As ν increases, isolas successively disappear in isola formation points or *isola centers* (Golubitsky & Schaeffer 1985, Ch.III, sect.3). See Fig. 7(b).

Using reasoning similar to that in Glendinning & Sparrow (1984, Sect. 3.1.2), it is possible to obtain asymptotic expressions as $\nu \to \nu_a$ for the ν-values at which isolas are either created or destroyed. Examining (3.1), note that isolas are created or destroyed when $\overline{z}(\nu, \mu_1, \sigma)$ reaches a turning point with

respect to σ at a point where the graph of the left-hand side of (3.1) is tangent to the graph of the right-hand side. Turning points of $\overline{z}$ with respect to σ occur at

$$\sigma = (1/2)(e\nu + f\mu_1), \tag{3.2}$$

and, from the form of (3.1), note that the tangency condition occurs when

$$(\omega/\lambda)\ln(z/\varepsilon) - \Phi_2 \approx -n\pi \ (n \in \mathbb{N}). \tag{3.3}$$

Taking n even in (3.3) corresponds to the creation of tangencies for $\nu > \nu_a$ and taking n odd corresponds to the destruction of tangencies for $\nu < \nu_a$. The approximation (3.3) is valid in the limit of large n, which corresponds to large-period. Let (z_n, ν_n, σ_n) be the (z, ν, σ)-values at the tangency corresponding to n in (3.3). Then (3.3) implies

$$z_n \approx \varepsilon \exp[-(\lambda/\omega)(n\pi + \Phi_2)]. \tag{3.4}$$

Also, noting that $\overline{z} = 0$ at $\nu = \nu_a$ by definition, we may write

$$\overline{z}(\nu_n) = \overline{z}'(\nu_a)(\nu_n - \nu_a) + \mathcal{O}((\nu_n - \nu_a)^2). \tag{3.5}$$

Also, at a z-value satisfying (3.3), the condition for a fixed point (3.1) simplifies to

$$\overline{z} = z_n \pm BF(\overline{x}, z_n, \mu_1).$$

This can be further simplified by expanding F as a Taylor series in the small parameter $w_n = (z_n/\varepsilon)^{-\delta}$ to obtain

$$\overline{z} = z_n \pm \frac{B\overline{x}}{\sqrt{D}}\left[w_n - \frac{\overline{x}^2}{\mu_1 D}w_n^3 + \mathcal{O}(w^4)\right], \tag{3.6}$$

where $D = 1 - (\overline{x}^2/\mu_1)$ and the plus sign corresponds to n even, the minus sign to n odd. Recall that $-1/2 < \delta < 0$. Hence the leading order term in the right-hand side of (3.6) for small z is the term proportional to w. Substituting from (3.4) and (3.5) into (3.6), to leading order one obtains

$$\overline{z}'(\nu_a)(\nu_n - \nu_a) \approx \pm B(\overline{x}/\sqrt{D})\exp[(\mu/\omega)(n\pi + \Phi_2)]. \tag{3.7}$$

From (3.7) it is apparent that the rate at isolas are created or destroyed as $\nu \to \nu_a$ is given by

$$\frac{\nu_{n+2} - \nu_a}{\nu_n - \nu_a} \to \exp\left[\frac{2\pi\mu}{\omega}\right] \quad \text{as } n \to \infty. \tag{3.8}$$

We make several observations concerning the formula (3.8).

1. First, note that it applies equally to isola creation and destruction upon taking n even or odd. Secondly, observe that the σ-values of isola creation and destruction, σ_n, obey exactly the same scaling owing to the linear relation (3.2) between $\sigma - \sigma_a$ and $\nu - \nu_a$.

2. Note further that nowhere in our analysis of isola creation and destruction have we used the fact that the equilibrium undergoes a Hopf-bifurcation (the analysis was carried out for fixed $\mu < 0$). Hence the formula (3.8) applies more generally to the formation of isolas near any non-transverse Shil'nikov homoclinic orbit which satisfies $|\delta| < 1/2$. The result could be arrived at more simply in this case, by using the simpler Poincaré map studied by Glendinning & Sparrow (1984). The key feature of both maps that leads to the relation (3.8) is that the right-hand side of (3.1) (or its equivalent) is dominated by the term $z^{-\delta}$ for small z.

3. Finally we note that (3.8) is identical to the asymptotic formula (Glendinning & Sparrow 1984, Eq. (12)) for the accumulation of saddle-node bifurcations on a codimension-one Shil'nikov homoclinic orbit.

We have not so-far mentioned the stability of periodic orbits. For $\nu < \nu_a$, when two Shil'nikov homoclinic orbits exist, the stability analysis of Glendinning & Sparrow (1984, Sect. 3.1.3) applies. Hence, each saddle-node bifurcation of periodic orbits of sufficiently large period, involves a saddle and a completely unstable orbit. This result is a consequence of $|\delta| < 1/2$. Note, however, that upon reversing time, the completely unstable periodic orbits become stable ones. Moreover, close to each saddle-node there must be a period-doubling bifurcation as depicted in 7(a). Using knowledge about isola formation and destruction, Fig. 7 also presents the conjectured results on the stability of periodic orbits as ν varies through ν_a, based on consistency with the Glendinning and Sparrow analysis for a single homoclinic orbit.

3.1.2 Supercritical region

We now study the situation for fixed $\mu = \mu_2 > 0$. Here the dynamics are qualitatively different depending on the relative signs of ν and $\nu_b(\mu_2)$, $\nu_c(\mu_2)$, where $\nu_b < 0$ and $\nu_c > 0$ are the two ν-values at which the apex of the locally quadratic curve (2.11) in (σ, ν) space occurs for fixed $\mu = \mu_2$. For fixed μ_2, this situation corresponds to a non-transverse homoclinic tangency to C (see Fig. 4). Specifically we have $\mu_2 = \mu_t^u(\nu_a)$ where μ_t^u is given by (2.12). The results of the graphical analysis of primary periodic orbits for this case are plotted in Fig. 8. In analogy with Fig. 7 we have also presented conjectures on the stability of the periodic orbits.

Note from the Figure that for $\nu < \nu_b$, each pair of homoclinic tangencies is approached by a primary periodic orbit in the manner predicted by the analysis of a non-degenerate Shil'nikov-Hopf bifurcation (Gaspard 1987, Hirschberg & Knobloch 1993). That is, the two periodic orbits in question each form a wiggly curve accumulating on the parameter values of two homoclinic tangencies. As ν increases, adjacent limbs of the two wiggly curves collide in transcritical bifurcations form isolas in the manner described in Fig. 7(a). The formation of isolas accumulates at $\nu = \nu_b$, the first non-transverse homoclinic tangency on increasing ν. Then for an interval of ν-values between the two tangencies, there exist infinitely many isolas. The bifurcation diagram for primary periodic orbits is now as described by Hirschberg & Laing (1995) in the unfolding of a non-transverse homoclinic tangency to a periodic orbit. Upon increasing ν further, beyond the value ν_c at which the two remaining homoclinic tangencies collide and dissapear, isolas start to disappear. The mechanism for disappearence is via succesive isolas shrinking to isola centers as in Fig. 7(b). The ν-values for isola destruction accumulate as $\nu \to \nu_c$ from below, so that there are at most finitely many isolas of primary periodic orbits for any fixed $\nu > \nu_c$, with a strict upper bound on their period.

3.2 Downward pointing case

The analysis of the downward pointing case is similar. We leave the details to the reader. In fact, the bifurcation behaviour of primary periodic orbits for fixed $\mu > 0$ and $\mu < 0$ is qualitatively the same as that in the upward pointing case, after redefinition of the ν-values of interest (cf. Figs. 4 and 5). For example, for $\mu_1 < 0$ where the origin is a saddle-focus, the non-transverse homoclinic orbit occurs for $\nu = \nu_a < 0$.

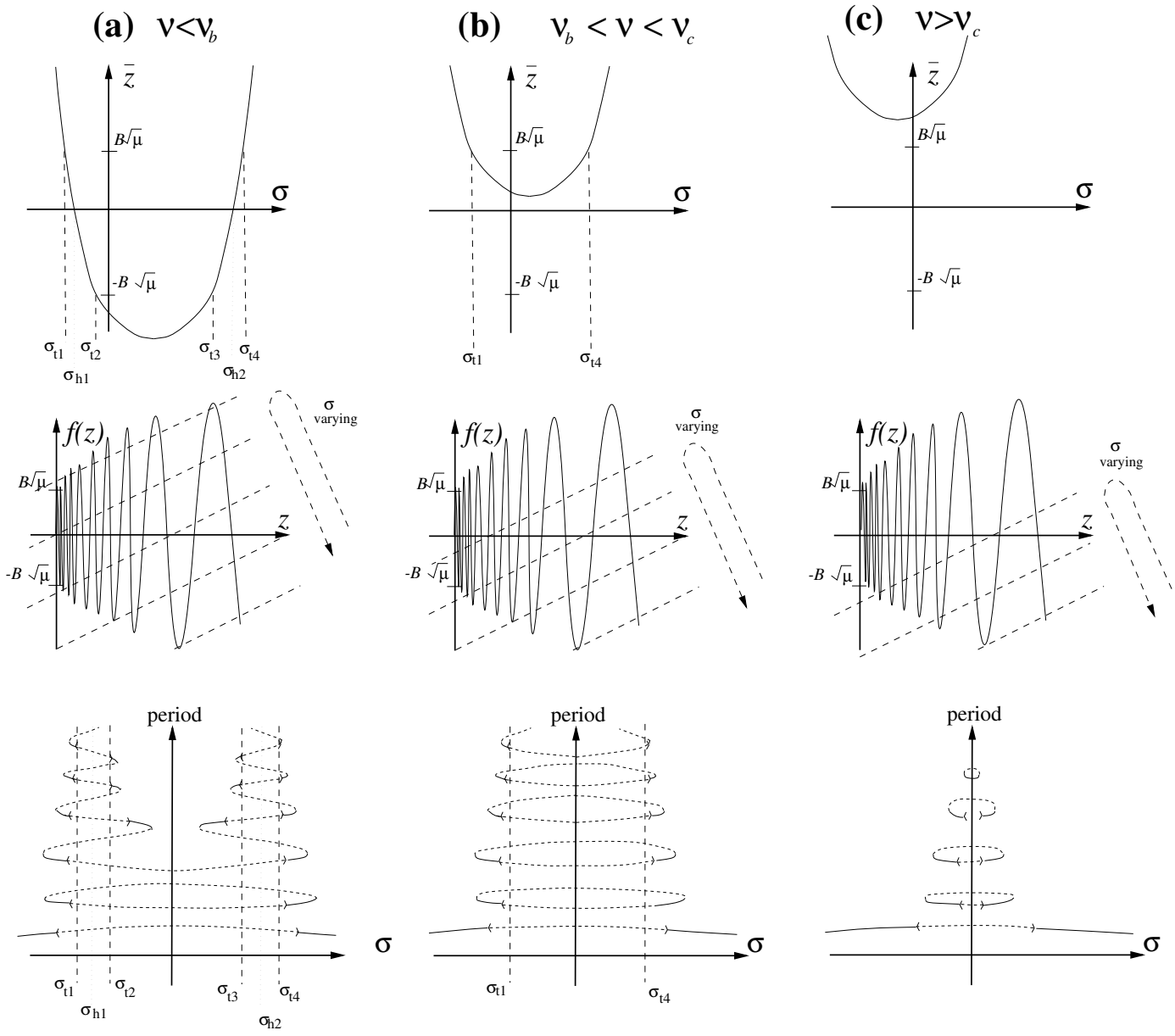

Figure 8: Depicting, analogously to Fig. 6, primary periodic orbits in the vicinity of homoclinic tangencies to C for fixed $\mu_2 > 0$ and three indicative values of ν. The marked σ-values σ_{ti} correspond to homoclinic tangencies to C and σ_{hi} to 0-to-C large heteroclinic orbits.

3.3 The effect of odd symmetry

Suppose that (2.1) has odd symmetry, that is, it is invariant under $\mathcal{S} : (x, y, z) \to (-x, -y, -z)$. Now, primary periodic solutions fall into two categories; symmetric orbits which are invariant under the symmetry and asymmetric orbits which are not and hence occur in symmetric pairs. Specifically a symmetric periodic orbit $\gamma(t)$ with period τ satisfies $\gamma(t+\frac{\tau}{2}) = -\gamma(t)$. One can now repeat the analysis of this section, on introducing two new Poincaré sections $-\Sigma_0$ and $-\Sigma_1$ which are the images of Σ_0 and Σ_1 under the symmetry. We do not give the details but refer instead to Glendinning (1984), who studies the case for a non-degenerate Shil'nikov homoclinic orbit, for indications of the necessary adaptations. Note, though, that the condition for a symmetric periodic orbit becomes that $\gamma(t) \in \Sigma_1 = -\gamma(t + \frac{\tau}{2}) \in -\Sigma_1$ and the expression so obtained bears a remarkable similarity to the condition (3.1) for an asymmetric periodic orbit. Since such a construction gives only half of a symmetric orbit, the period of the symmetric orbits constructed in this way will be approximately twice that of the corresponding asymmetric orbit. Also, symmetric orbits cannot period double (see, for example, Kuznetsov (1995)[Sect. 7.4]) hence the analogue of period doubling bifurcations on wiggly curves for symmetric periodic orbits should be interpreted as symmetry breaking (pitchfork) bifurcations.

The results of the graphical analysis in the odd symmetric case is presented in Fig. 9, which shows the analogues of Figs. 6 and 8. Note that the ordinate should be interpreted as the period of an asymmetric orbit and half the period for symmetric orbits. Recall also that a curve of asymmetric orbits represents two orbits, which are images of each other under $\mathcal{S}$. The stability of the periodic orbits in Fig. 9 is not depicted but is similar to that in Figs. 7 and 8, upon recalling that period-doubling is replaced by symmetry-breaking for symmetric orbits.

4 A numerical example

4.1 An autonomous nonlinear electronic circuit

The electronic circuit we consider is genealogically related to the classical Rayleigh and van der Pol oscillators. Its scheme is shown in Fig. 10, and it represents a coupling, by means of a resistor G_2, of two elementary circuits; a parallel RCL-circuit (a resistor G_3, an inductor L and a capacitor C) and an RC-circuit (a resistor G_1 and a capacitor C_0). Taking the voltages on the capacitors and the current across the inductor as state variables, modelling the current-voltage characteristics of resistors G_1, G_2 and G_3 by cubic odd functions and after some rescaling of time, state variables and parameters, the corresponding state equations of this circuit are

$$\begin{aligned} \dot{x} &= -\frac{(\nu+\beta)}{r}x + \frac{\beta}{r}y - \frac{a_3}{r}x^3 + \frac{b_3}{r}(y-x)^3, \\ \dot{y} &= \beta x - (\beta+\gamma)y - z - b_3(y-x)^3 - c_3y^3, \\ \dot{z} &= y. \end{aligned} \tag{4.1}$$

(Nb. ν here is unrelated to the unfolding parameter ν used earlier).

The dynamics of (4.1) have been studied by a number of authors. It is invariant under the $\mathbb{Z}_2$-symmetry

$$(x, y, z) \to (-x, -y, -z),$$

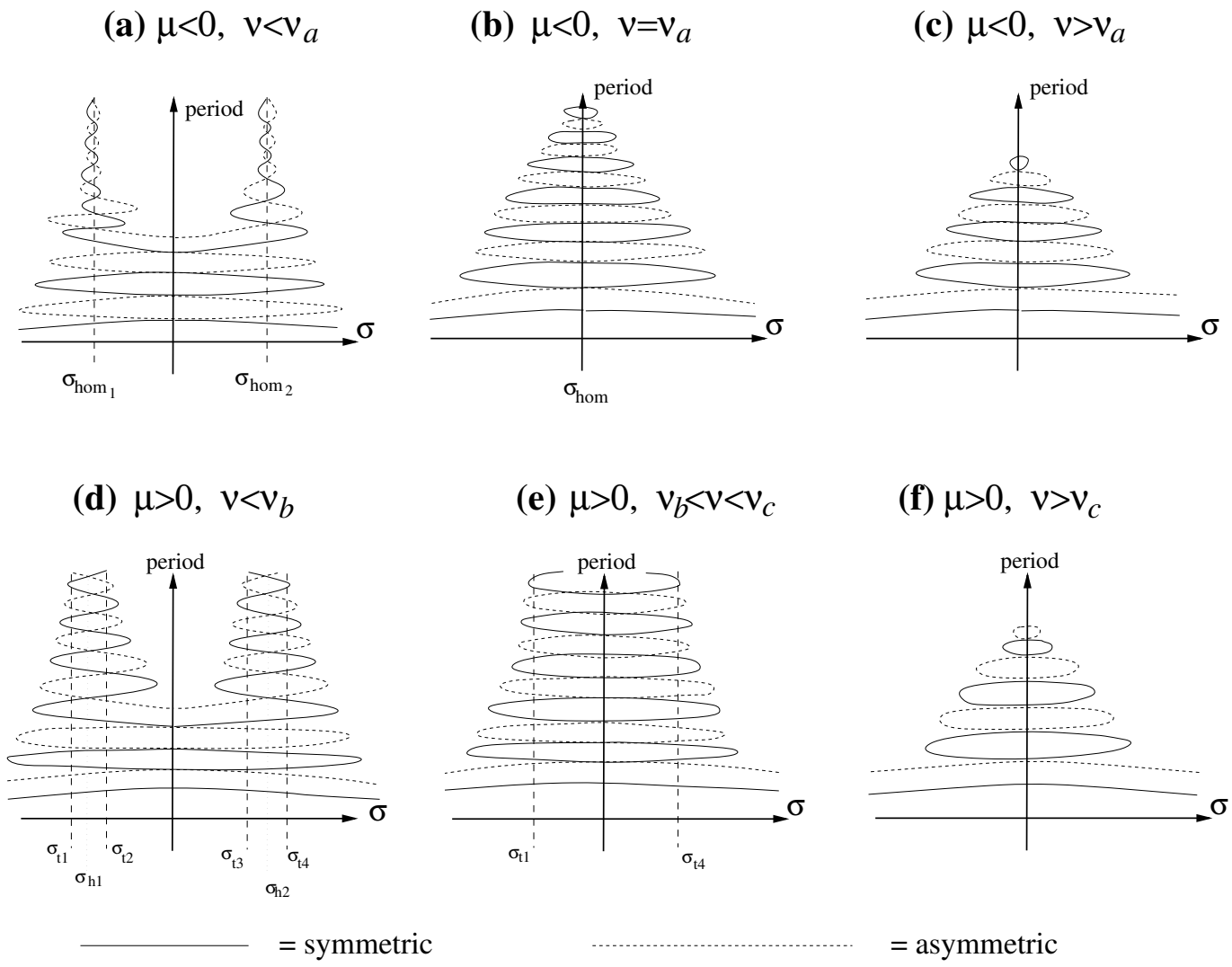

Figure 9: Depicting primary periodic orbits analogously to Figs. 7 and 8 in the case of odd symmetry. Dashed lines indicate symmetric orbits and solid lines represent asymmetric orbits.

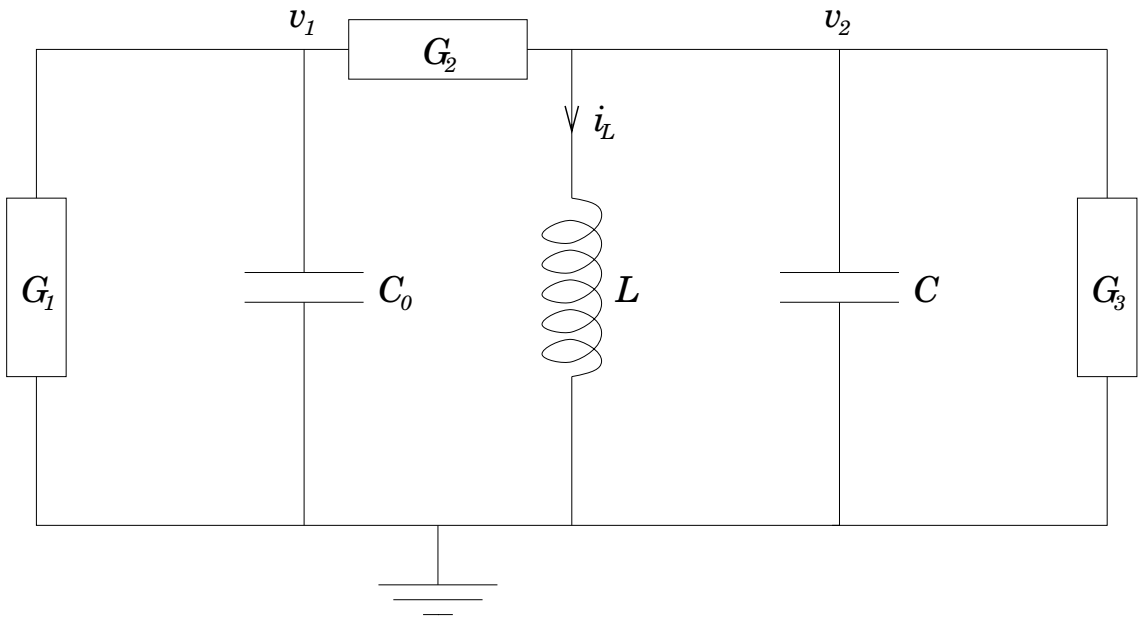

Figure 10: A schematic diagram of the electronic circuit, containing three resistors (G_1, G_2 and G_3), two capacitors (C_0 and C) and an inductor (L). The state variables x, y and z correspond respectively to the voltages across the capacitors v_1 and v_2 and the current across the inductor (i_L) appropriately rescaled.

and hence the origin is always an equilibrium. When $\nu + \beta < 0$, $a_3 + b_3 > 0$, a pair of asymmetric equilibria also exist. Local bifurcations of these equilibria (pitchfork, Hopf, Bogdanov-Takens, Hopf-zero) have been studied in previous works; see Freire et al. (1993), Algaba, Freire, Gamero & Rodríguez-Luis (1998) and references therein. The presence of a triple-zero degeneracy is also summarized in Freire et al. (1993) and its normal form is computed in Gamero, Freire, Rodríguez-Luis, Ponce & Algaba (1993). Also in Freire et al. (1993), a global parameter-space investigation was undertaken in the (ν, β)-plane with the other parameters fixed at the values

$$r = 0.6, \quad a_3 = 0.328578, \quad b_3 = 0.933578, \quad c_3 = 0 \tag{4.2}$$

and $\gamma = 0$. It was shown numerically that a branch of (a symmetric pair of) homoclinic orbits to the origin could be traced from the Bogdanov-Takens (BT) bifurcation of the origin at $(\nu, \beta) = (-\sqrt{0.6}, \sqrt{0.6})$ to a Shil'nikov-Hopf bifurcation at $(\nu, \beta) = (-1.026452, 0)$. See Fig. 11(a) below, where the BT point in this and similar subsequent figures occurs at top of the figure where one of the homoclinic branches terminates 'in mid air'. This branch of homoclinic solutions that bifurcates from small amplitude at the BT point we shall refer to as the *primary* solution branch and any other homoclinic orbits to the origin (as on the other curve of homoclinic solutions in Fig. 11(a)) as being *secondary*.

Fernández-Sánchez, Freire & Rodríguez-Luis (1997*a*) consider several additional codimension-two global bifurcations that are obtained upon varying γ. It is discovered that for γ sufficiently negative the homoclinic orbit originating in the BT point when followed in the (ν, β)-plane ends not at a Shil'nikov-Hopf point but at a so-called T-point (Bykov 1993, Glendinning & Sparrow 1986) formed by the existence of a heteroclinic cycle between the origin and the asymmetric equilibria. See Fig. 11(d) below for the homoclinic locus and 12(c) for a phase portrait of the heteroclinic cycle at the T-point. It is argued in Fernández-Sánchez, Freire, Gamero & Rodríguez-Luis (1997) and Fernández-Sánchez, Freire

& Rodríguez-Luis (1997*a*) that in making the transition between these two cases (Figs. 11(a)–(d)) the system must undergo infinitely many non-transverse Shil'nikov-Hopf bifurcation points. These non-transverse bifurcations accumulate on parameter values at which the T-point and the locus of Hopf bifurcations of the origin coincide (estimated to occur for $\nu \approx -0.861$, $\beta \approx 0.109$, $\gamma \approx -0.1187$).

Furthermore, due to the $\mathbb{Z}_2$-symmetry and the saddle-focus character of the three equilibria involved in the heteroclinic cycle, three spiraling curves in the parameter plane emerge from the T-point. These curves represent homoclinic orbits to the origin, homoclinic orbits to the nontrivial equilibria and heteroclinic connections between the nontrivial equilibria. All three curves may end sometimes at Hopf bifurcations (of the origin or of the non-symmetric equilibria) giving rise to three kinds of Shil'nikov-Hopf singularities. Furthermore, numerical continuation of principal and secondary T-points suggests that all these curves end at codim 3 (T-point+Hopf)-points. This strongly suggests that (4.1) possesses infinitely many nontransverse Shil'nikov-Hopf bifurcations to asymmetric equilibria as well as symmetric ones: see Fernández-Sánchez, Freire, Gamero & Rodríguez-Luis (1997) and Fernández-Sánchez, Freire & Rodríguez-Luis (1997*a*) for the details.

Here we are interested only in the non-transverse Shil'nikov-Hopf points and their implications on the bifurcation diagrams of periodic orbits. Throughout we shall take ν, β, and γ as our unfolding parameters with the other parameters fixed at the values (4.2).

In what follows we shall use the software AUTO (Doedel, Keller & Kernévez 1991, Doedel, Champneys, Fairgrieve, Kuznetsov, Sandstede & Wang 1997) to compute branches of periodic and homoclinic orbits. In order to compute branches of homoclinic orbits, we use the algorithms described in Champneys & Kuznetsov (1994) and Champneys, Kuznetsov & Sandstede (1996). Using those methods, one can: accurately detect Shil'nikov-Hopf bifurcation points at the termination of a branch of homoclinic orbits; continue a branch of large point-to-periodic heteroclinic orbits beyond the codimension-two point and; continue a path of Shil'nikov-Hopf points as three parameters are varied. In addition, we shall also compute approximations to branches of homoclinic tangencies by following, in two parameters, saddle-node bifurcation points of periodic orbits with high period on wiggly curves accumulating at homoclinic tangencies. See Fig. 8(a) for why this is a valid approximation. This latter method was suggested to us by E. Doedel and its effectiveness will form the subject of future work.

4.2 Upward-pointing bifurcation to a symmetric equilibrium

Fig. 11 shows what happens to two loci of homoclinic orbits as γ is decreased from zero. Note from Figs. 11(c) and (d) that for a value of $\gamma \in (-0.65, -0.5)$ a tangency must occur between the curve of homoclinic orbits and Hopf bifurcations. Fig. 12 shows the phase portrait projections of a saddle-focus homoclinic orbit, a point-to-periodic heteroclinic orbit and a T-point. Fig. 13 shows the result of three-parameter continuation in (ν, β, γ) of the two Shil'nikov-Hopf bifurcation points found for $\gamma = 0.5$. A non-transverse Shil'nikov-Hopf bifurcation occurs at $(\nu, \beta, \gamma) = (-0.633130, 0.459758, -0.592060)$, the limit point with respect to γ in Fig. 13(a). Note that this corresponds to the upward-pointing case in our notation. Fig. 14 shows four homoclinic orbits along the locus of Shil'nikov-Hopf points.

In order to illustrate the preceding analysis of periodic orbits in the upward pointing case with $\mathbb{Z}_2$-symmetry, we first consider asymmetric periodic orbits. We fix $\gamma = -0.65$ and consider three horizontal slices through Fig. 11(d), by allowing β to take three different values. The results are presented in Fig. 15. For the first β-value, 0.64, the asymmetric periodic orbits emanating from the two homoclinic orbits depicted in Fig. 11(d) are *not* found to lie on the same branch. Instead, one branch forms a connection between two homoclinic orbits to the origin (one of which is not represented in Fig. 11(d)) and the

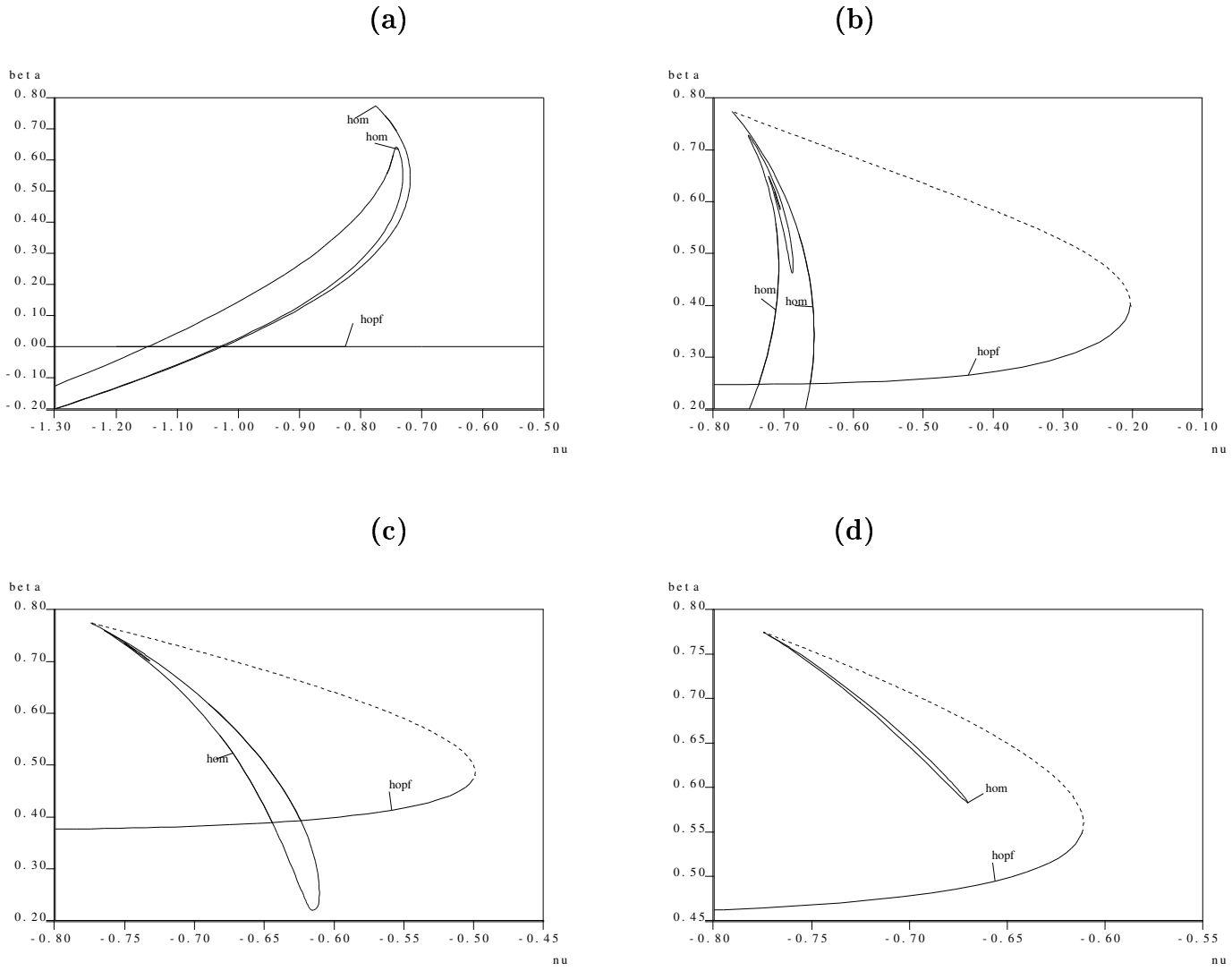

Figure 11: Curves `hom` of primary homoclinic orbits to the origin and `hopf` of Hopf bifurcations of the origin (dashed = sub-critical, solid=super-critical) for (a) $\gamma = 0$, (b) $\gamma = -0.3$, (c) $\gamma = -0.5$, (d) $\gamma = -0.65$. Below the Hopf bifurcation line, the curve `hom` represents large point-to periodic heteroclinic orbits.

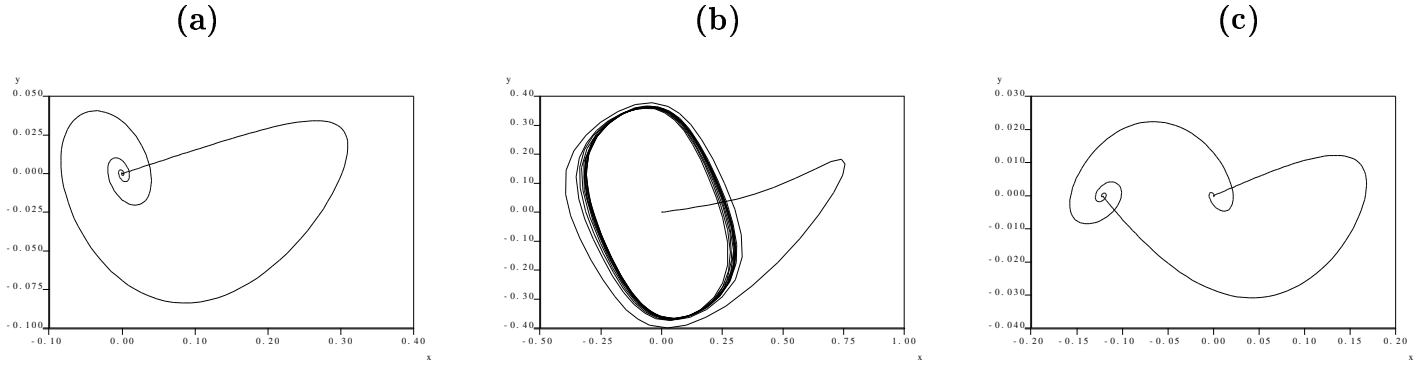

Figure 12: Phase portrait projections of solutions for $\gamma = -0.5$. (a) saddle-focus homoclinic orbit at $(\nu, \beta) = (-0.689935, 0.618709)$, (b) point-to-periodic heteroclinic orbit at $(\nu, \beta) = (-0.615438, 0.220275)$, (c) T-point at $(\nu, \beta) = (-0.743288, 0.726500)$.

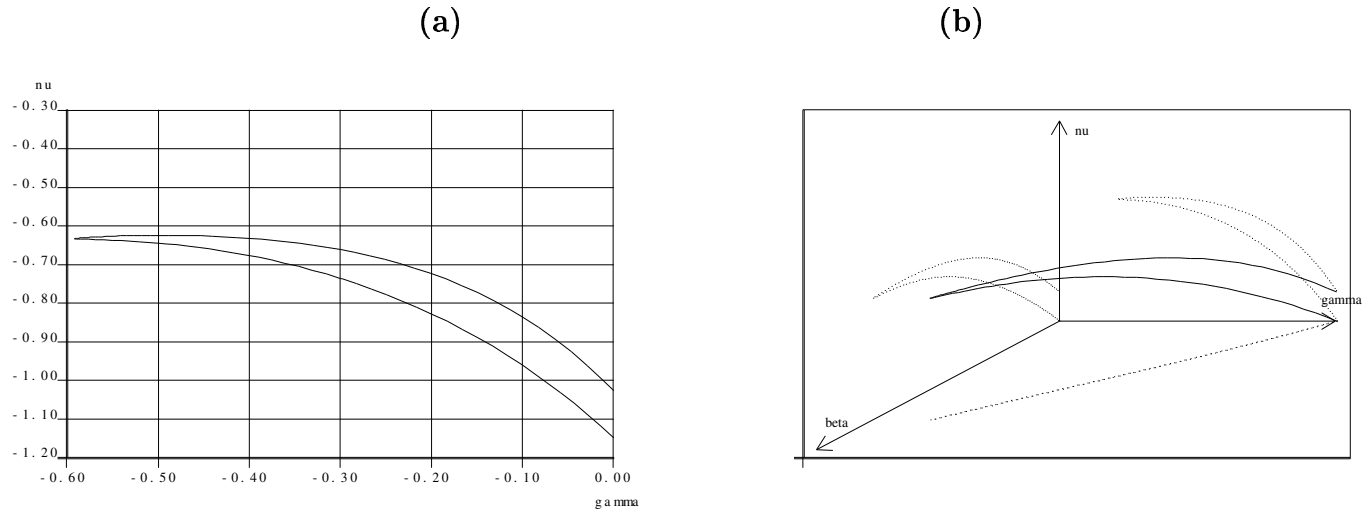

Figure 13: Curve of Shil'nikov-Hopf bifurcations showing the non-transverse Shil'nikov-Hopf bifurcation as a limit point: (a) a two-parameter projection; (b) in three-parameter space.

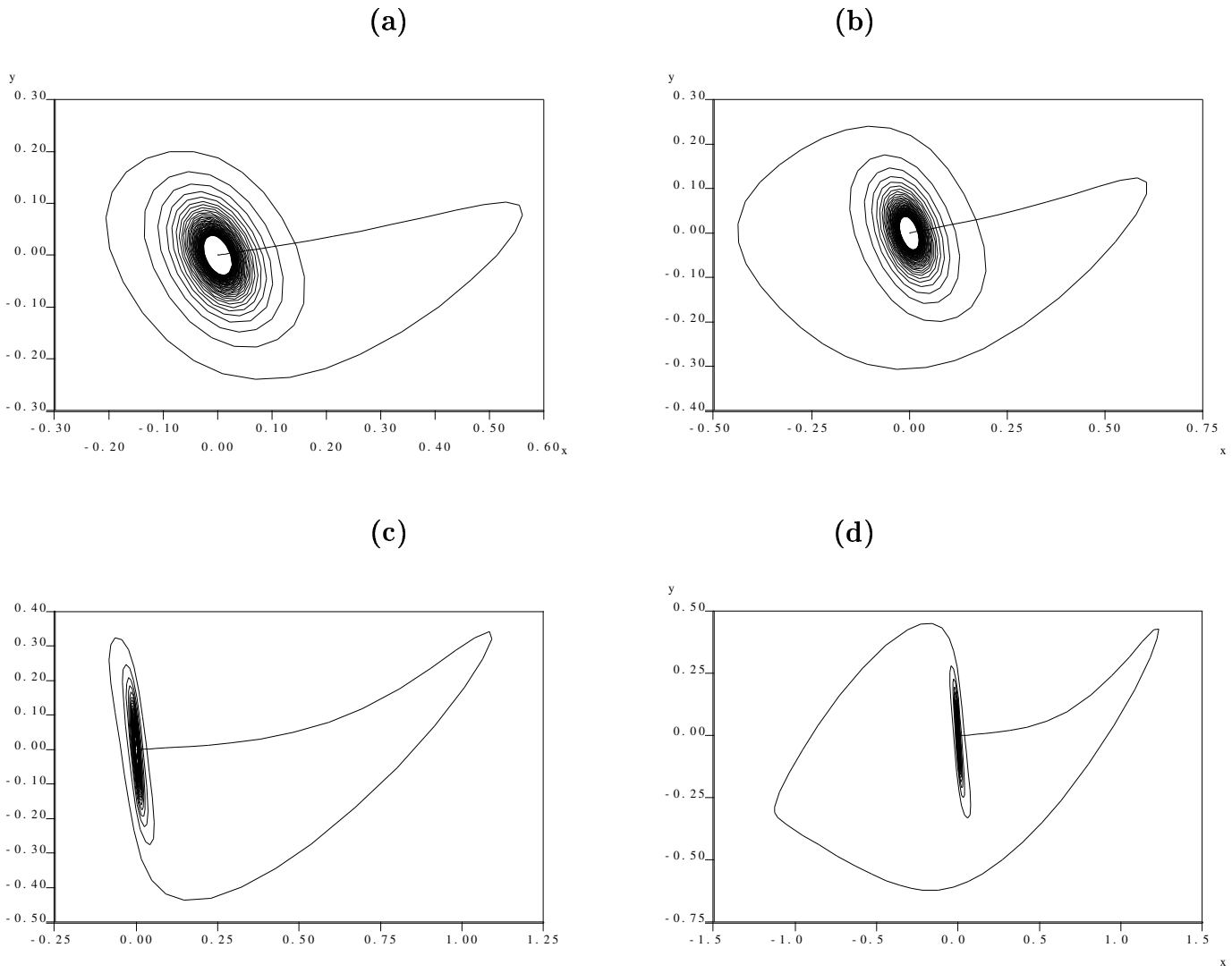

Figure 14: Phase portraits of homoclinic orbits on the Shil'nikov-Hopf locus depicted in Fig. 13. (a) The primary orbit for $\gamma = -0.5$, (b) the secondary orbit for $\gamma = -0.5$, (c) the primary orbit for $\gamma = -0.1$, (d) the secondary orbit for $\gamma = -0.1$.

other forms a connection between a homoclinic to the origin and a homoclinic orbit to the nontrivial equilibria. See Fig. 16 for the phase portrait projections of these four different large period limits. At the moment, these bifurcation diagrams do not correspond well with the theory of Section 3.

For the next β-slice depicted in Fig. 15(b), $\beta = 0.62$ which is close to the turning point of the homoclinic locus in Fig. 11(d), now the two homoclinic orbits on the primary locus *are* connected by a single branch of asymmetric periodic orbits. The bifurcation diagram is quite like that predicted by the theory in Fig. 7(a). There are two isolas for small period, and the two wiggly curves approaching the two homoclinic orbits are connected.

As β is further decreased to approximately the tip of the homoclinic locus in Fig. 11(d), the two wiggly curves can be seen to annihilate each other by forming more and more isolas, in a process like that depicted in Fig. 7. E.g. Fig. 15(c) shows that for $\beta = 0.58$ we observe the first eight isolas in the evident destruction process. Note however, that the isola creation and destruction process is not entirely the same as predicted by the theory since the isolas here are not approximately circular at least not until they are of very small diameter. Comments on the causes of this discrepancy will be made in the Conclusion. In the meantime, observe from Fig. 17 the detail of an isola formation for $\gamma = -0.6$ and two very close values of β. Stability of the periodic orbits is sketched in Fig.15 (d) and (e).

As predicted by the theory, symmetric periodic orbits also exhibit a process of isola creation/destruction. To illustrate it we show in figure 18 the bifurcation diagram for $\gamma = -0.65$ and two values of β. When $\beta = 0.64$ the two branches are connected and there are no isolas. Decreasing this parameter to $\beta = 0.62$, observe that a first isola has been created.

Finally we move to $\gamma = -0.5$, on the other side of the codimension-three point, where the homoclinic orbit and homoclinic tangency are no longer disconnected, and attempt to look for complex behaviour in the vicinity of homoclinic tangencies. The results are presented in Figs. 19 and 20. Fig. 19(a) shows a bifurcation diagram with ν of asymmetric periodic orbits for $\beta = 0.44$, above the Hopf bifurcation line. Here two homoclinic orbits are joined by a curve of periodic orbits as described in Fig. 6(a). Fig. 19(d) then shows loci in the (ν, β) parameter plane of the saddle-nodes which accumulate on the leftmost of these homoclinic orbits. Note that some of these curves cross the Hopf-bifurcation line. The innermost saddle-node below the Hopf line describes approximately the locus of homoclinic tangencies (as in Fig. 8(a)). Note also the strange accumulation of cusps to the right in Fig. 19(d). The saddle-node curves corresponding to the rightmost homoclinic orbit in Fig. 19(a) describe qualitatively similar curves in the (ν, β) plane.

Fig. 20 shows a one-parameter bifurcation diagram of the asymmetric periodic orbits partially below the Hopf line (for $\beta = 0.39665$) starting from one of the computed saddle-node curves. Notice here the complication that one end of the branch ends in a heteroclinic connection to the asymmetric equilibrium, plotted in Fig. 20(d). This heteroclinic connection (which may well explain the cusps in Fig. 19(d)) is providing an extra complication to the dynamics which is hampering our ability to trace out numerically curves of homoclinic tangencies.

Further numerical experimentation closer to the codim 3 point (e.g. at $\gamma = -0.59$) have so far failed to resolve the behaviour of the locus of homoclinic tangencies.

4.3 Downward-pointing bifurcation to a symmetric equilibrium

Next we consider bifurcation diagrams of asymmetric periodic orbits for the downward pointing case. In order to find such a situation we need to increase γ still further, because for $\gamma = -0.1187$ the T-point is found to coalesce with the Hopf bifurcation of the origin (Fernández-Sánchez, Freire, Gamero

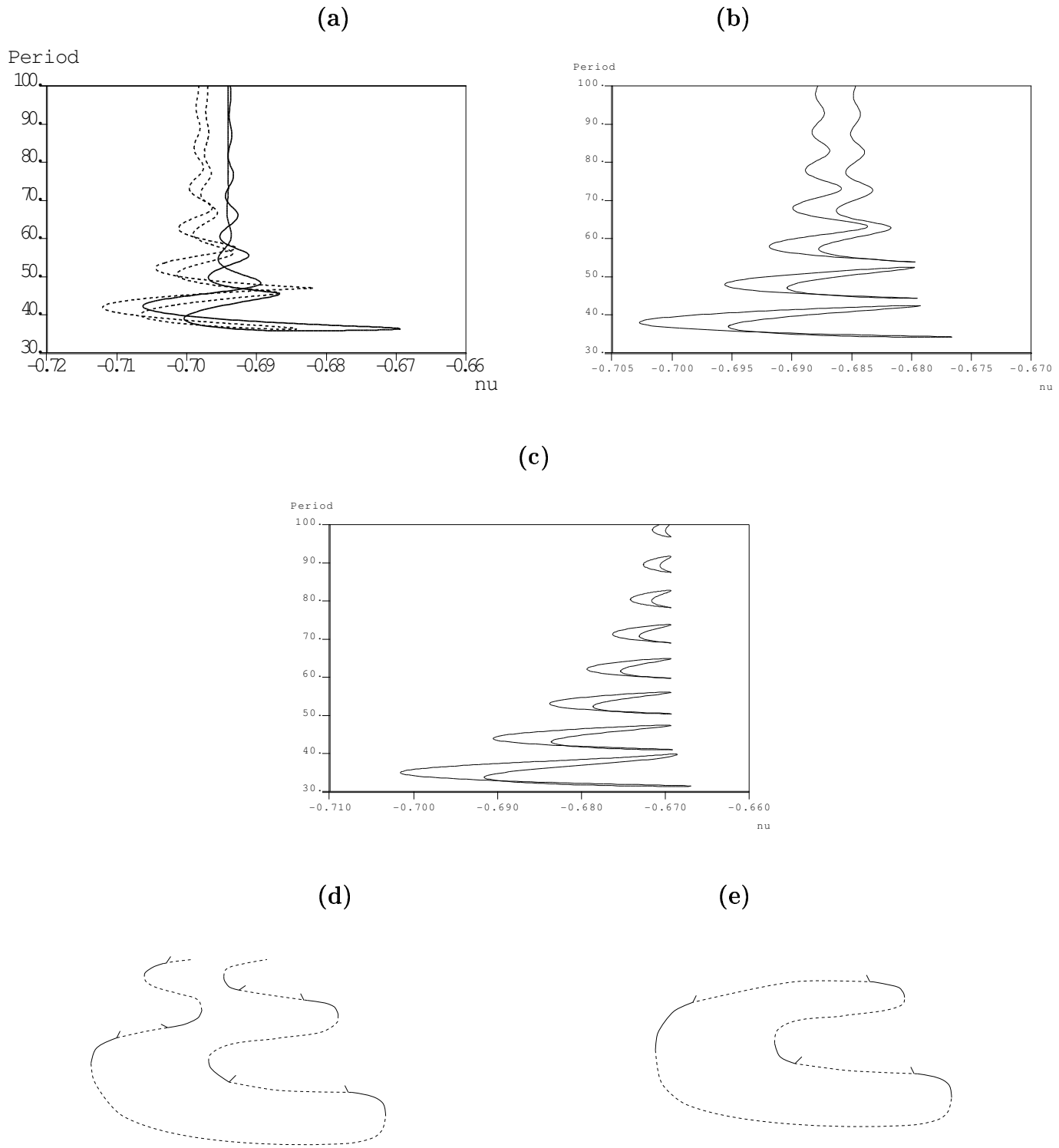

Figure 15: Bifurcation diagrams for asymmetric periodic orbits in the upward pointing case for $\gamma = -0.65$: (a) $\beta = 0.64$ (to distinguish one branch to the other, the left one is dashed); (b) $\beta = 0.62$; (c) $\beta = 0.58$. The stability of the orbits is sketched in (d) and (e). Broken lines indicate saddle orbits and solid lines unstable orbits; flip bifurcations are marked with slanted segments.

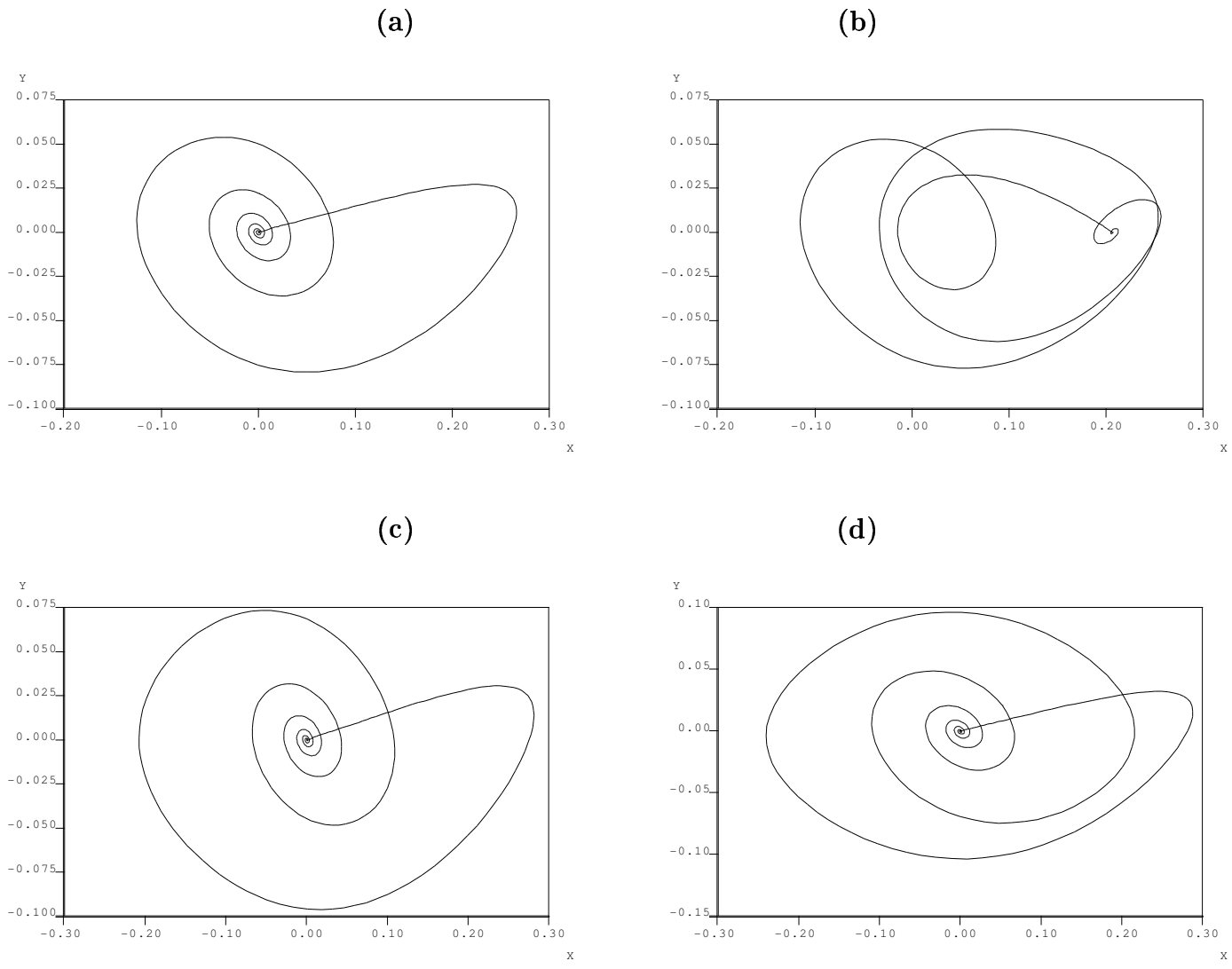

Figure 16: Phase portraits of periodic orbits in the four branches in Fig. 15(a), from the right branch (a) to the left one (d).

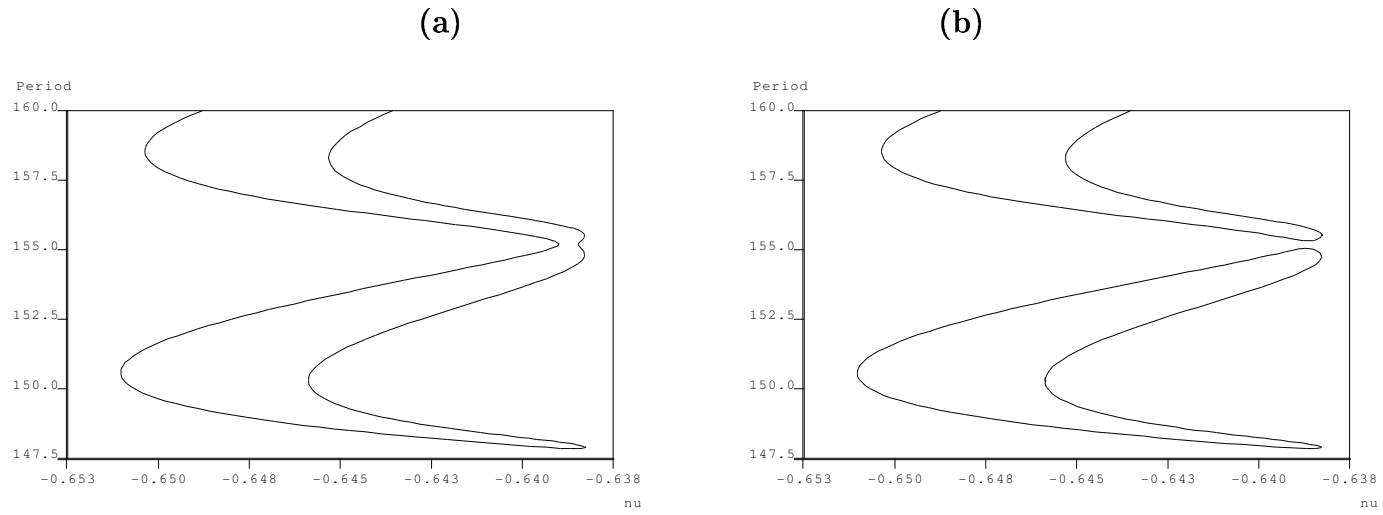

Figure 17: Detail of an isola formation for asymmetric periodic orbits in the upward pointing case for $\gamma = -0.6$: (a) $\beta = 0.5$; (b) $\beta = 0.4999$.

& Rodríguez-Luis (1997)). At this γ-value, only the upper half of the spiralling homoclinic curve in the (ν, β) plane persists. The infinitely many points at which this intersects the Hopf line each correspond to Shil'nikov-Hopf points. Therefore, for γ values close to -0.1187 there must be an infinite sequence of parameter values at which non-transverse Shil'nikov-Hopf bifurcations occur.

We decrease γ beyond this special value to $\gamma = 0$, at which value we depict in Fig. 21(a), three branches of the remanants of the spiral of homoclinic solutions – the Hopf bifurcation of the origin corresponds to $\beta = 0$. (To better understand this figure, see also Fig. 3 in Freire et al. (1993).) Hence there are six Shil'nikov-Hopf points of homoclinic orbits to the origin.

Focussing on the inner branch, Fig. 22 shows bifurcation diagrams for several constant β-values, where the isola creation/destruction process is evident as it was in the upward pointing case described in the previous subsection. Note, in comparison with Fig. 15, that the agreement with the theoretical shapes of the isolas in Fig. 7 seems somewhat better here, especially for higher period. The phase portraits of all these periodic orbits are similar to the homoclinic connection in Fig. 21(d).

4.4 Shil'nikov-Hopf bifurcation to an asymmetric equilibrium

Fig. 23 depicts a branch of Shil'nikov-Hopf bifurcations to an asymmetric equilibrium, showing the existence of a non-transverse Shil'nikov-Hopf point. Owing to the very narrow γ-interval between the two Shil'nikov-Hopf points for given ν, we do not attempt to investigate the dynamics in a neighbourhood of this codim 3 point.

5 Conclusion

In this paper we have outlined heuristically the behaviour of the simplest possible homoclinic and periodic orbits in a neighbourhood of a bifurcation causing the disconnection between a branch of homoclinic orbits and homoclinic tangencies. Our analysis was motivated by the observation that this bifurcation must occur infinitely many times in the nonlinear electronic circuit example studied in Section 4. Indeed using careful direct computation, we have managed to isolate the parameter

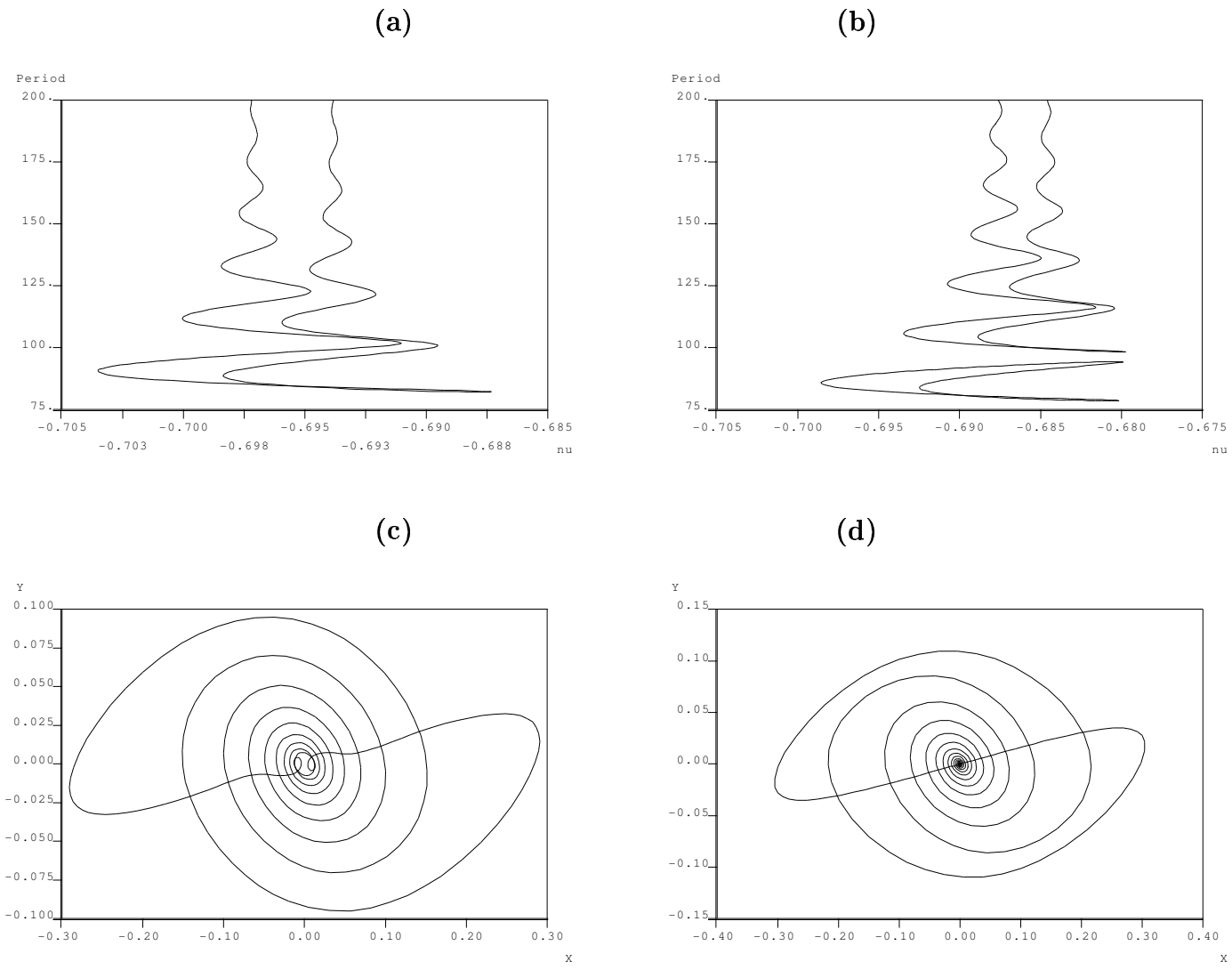

Figure 18: Bifurcation diagrams for symmetric periodic orbits in the upward pointing case for $\gamma = -0.65$: (a) $\beta = 0.64$; (b) $\beta = 0.62$; (c) and (d) phase portraits of these orbits in both branches for $\beta = 0.62$.

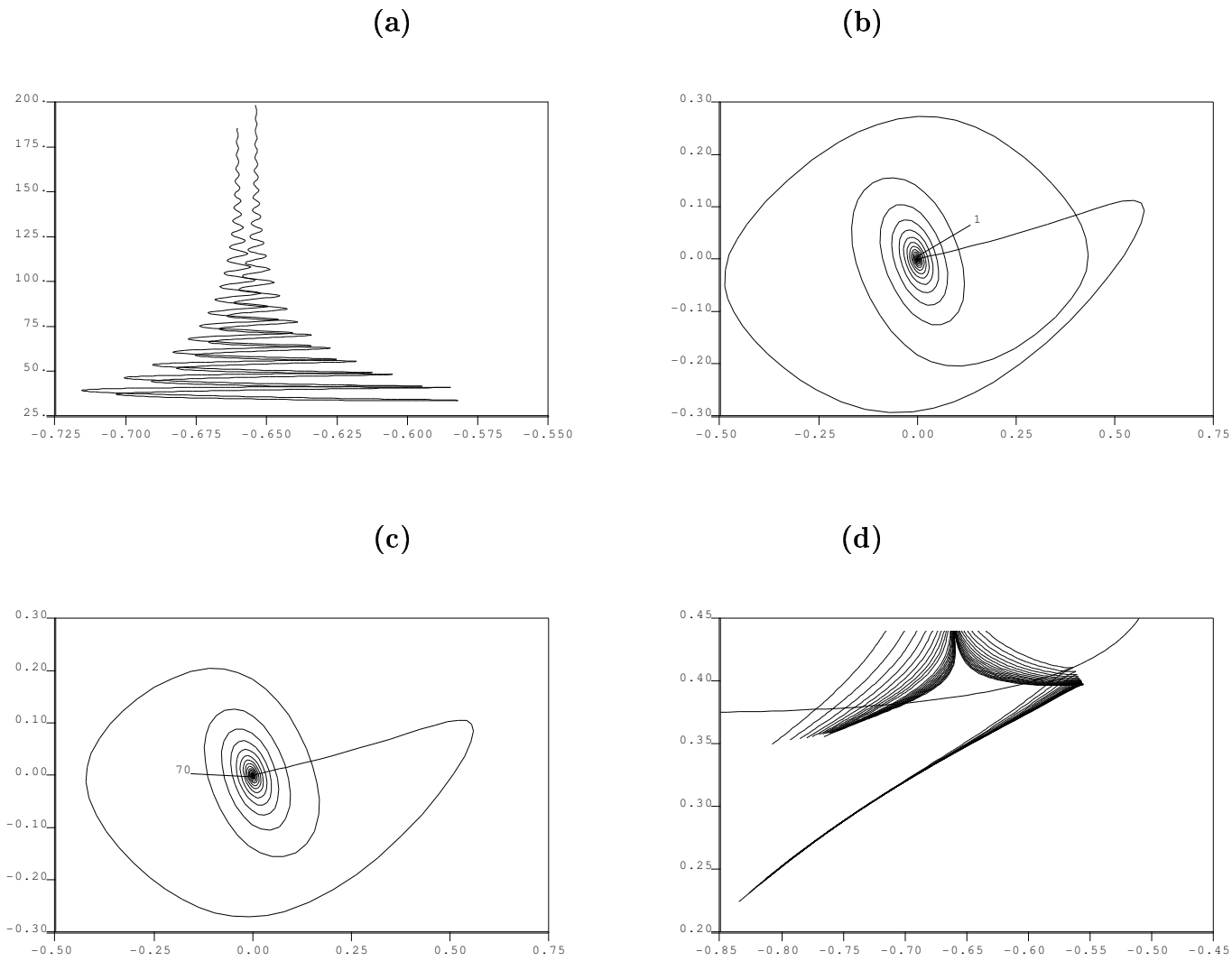

Figure 19: Bifurcation diagram for $\gamma = -0.5$: (a) ν-Period bifurcation diagram for $\beta = 0.44$; (b) and (c) x-y projections of periodic orbits close to the homoclinic orbits at the endpoints of both branches. (d) Curves in the ν-β plane of saddle-node points of the left branch in (a) with the curve of Hopf bifurcations of the origin superimposed.

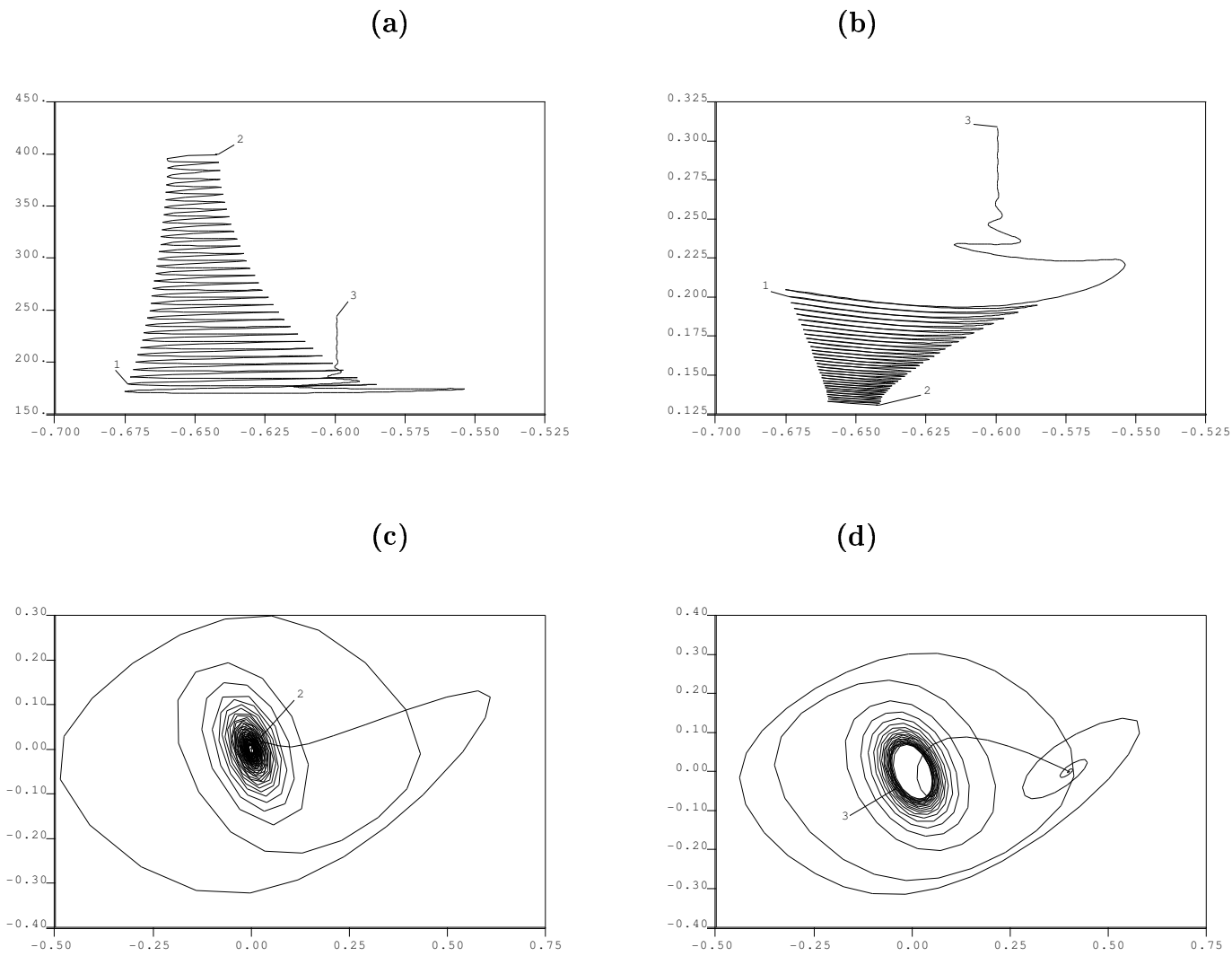

Figure 20: Bifurcation diagram for $\gamma = -0.5$ and $\beta = 0.39665$: (a) ν-Period; (b) ν-norm; (c) and (d) x-y projections of the labeled periodic orbits.

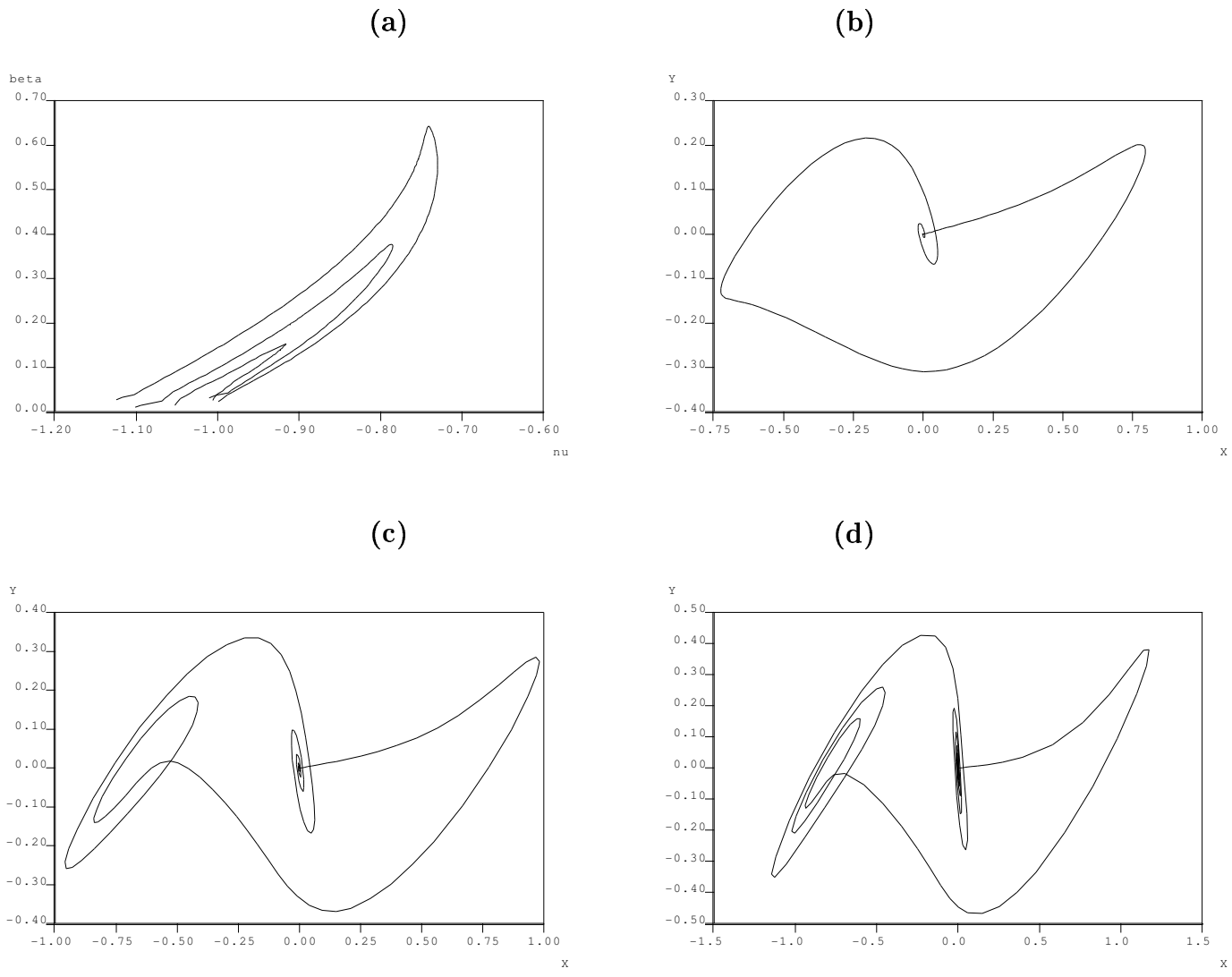

Figure 21: Homoclinic orbits to the origin for $\gamma = 0$: (a) three branches in the ν-β parameter plane; (b)-(d) phase portraits of homoclinic orbits in (b) the outer branch, (c) the middle branch and (d) the inner branch.

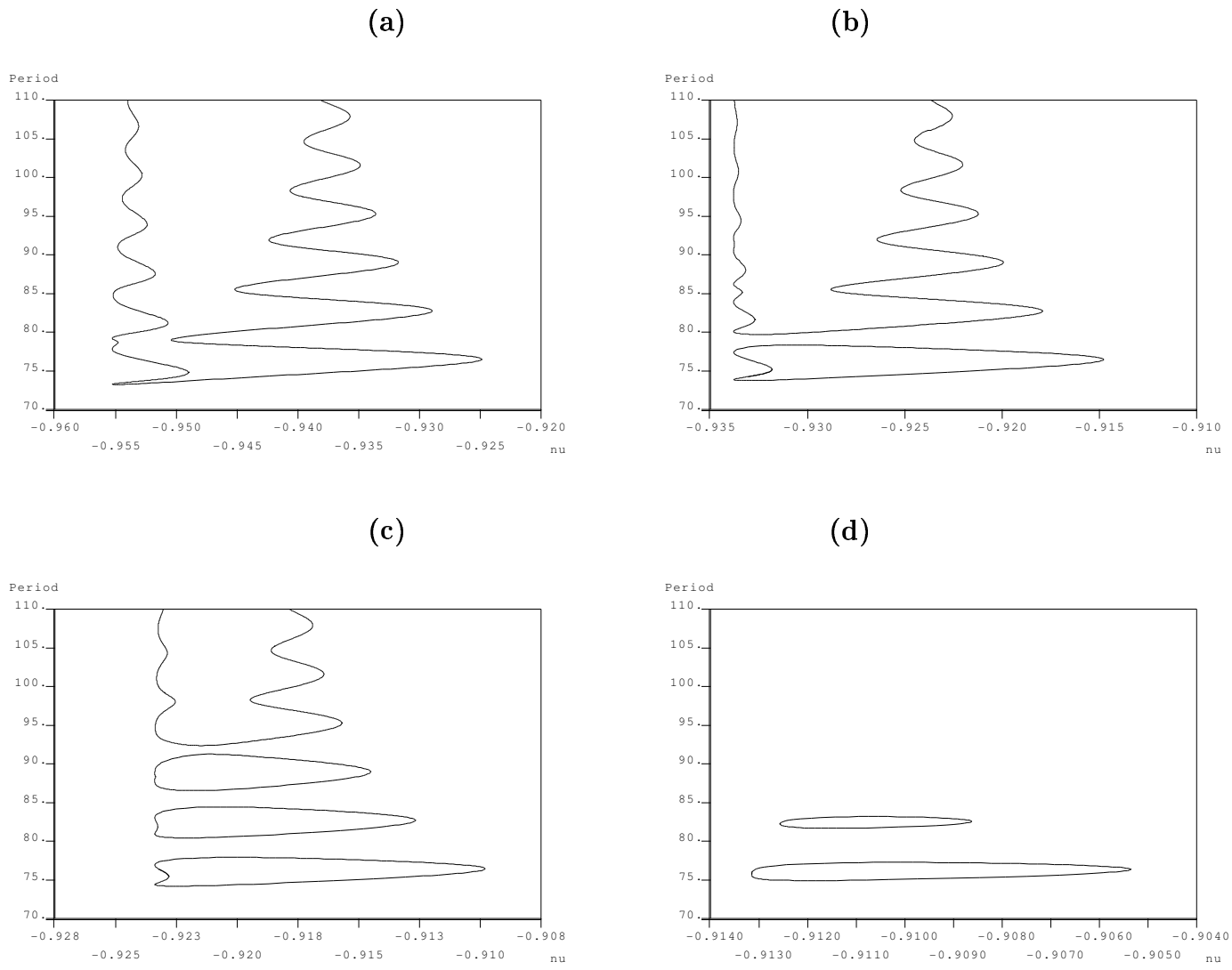

Figure 22: Bifurcation diagrams for asymmetric periodic orbits in the downward pointing case for $\gamma = 0$: (a) $\beta = 0.12$; (b) $\beta = 0.14$; (c) $\beta = 0.15$; (d) $\beta = 0.16$.

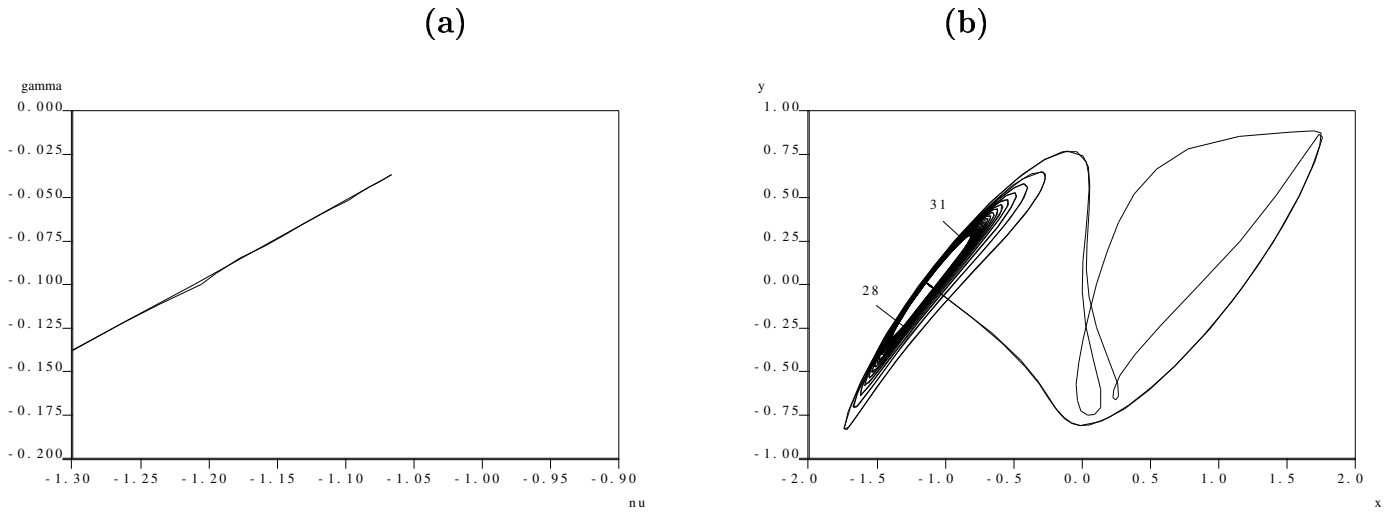

Figure 23: (a) A two-parameter projection of the curve of Shil'nikov-Hopf bifurcations to an asymmetric equilibrium showing the non-transverse Shil'nikov-Hopf bifurcation as a limit point. (b) Two Shil'nikov-Hopf homoclinic orbits for $\gamma = -0.1$.

values at which three different types of non-transverse Shil'nikov-Hopf bifurcations occur; upwards and downwards pointing, and involving symmetric and asymmetric equilibria.

For the behaviour of the periodic orbits in a neighbourhood of the degeneracies at the symmetric equilibria, some agreement was found between the numerics and the theory; for example the creation and destruction of isolas of periodic orbits shown in Figs. 15 and 22. We remark on the discrepancies between the shapes of these isolas and those predicted by the simple theory of Section 3 (see Figs. 7 and 9). Fernández-Sánchez, Freire & Rodríguez-Luis (1997*b*) have conducted a thorough investigation of the behaviour of a particular isola of asymmetric periodic orbits in the same electronic circuit (4.1), albeit at different parameter values. Upon varying certain parameters, isolas of periodic orbits were found to be created or destroyed in mechanisms similar to those outlined in Fig. 7 (with the transcritical bifurcation in Fig. 7(a) replaced by a pitchfork with a slightly more complicated unfolding). In addition they found a further cusp point at which isolas with two saddle-node bifurcations obtained two extra saddle-nodes; cf. the transitions which appear to be occuring in Fig. 22.

Clearly the example system has more structure than that assumed for the general system we analyse in Sects. 2 and 3, not least due to heteroclinic connections to the two asymmetric equilibria. In fact, extra winding around these equilibria may account for the additional saddle-nodes on the isolas. However. these heteroclinic orbits have a more fundamental role in the observed unfolding of the non-transverse Shil'nikov-Hopf bifurcations, as illustrated by Fig. 20. Here, instead of a single curve of primary periodic orbits connecting two homoclinic tangencies to the small periodic orbit as in Fig. 8(a), we find that a homoclinic tangency is connected to a *heteroclinic* connection between the asymmetric equilibrium and the weak unstable manifold of the equilibrium. Part of the problem here is that the model parameter β does not play precisely the role of the unfolding parameter σ, but also varies the distance to the Hopf bifurcation. Furthermore, the role of the T-point colliding with the Hopf bifurcation locus has already been mentioned in organising an infinite accumulation of non-transverse Shil'nikov Hopf bifurcations. Some of the additional complexities are clearly better explained by unfolding that degeneracy, but it is remarkable complicated (Fernández-Sánchez, Freire, Gamero & Rodríguez-Luis 1997, Fernández-Sánchez, Freire & Rodríguez-Luis 1997*a*).

A slight disappointment is that we have so far been unable to numerically trace out accurate loci in two-parameters of homoclinic tangencies to periodic orbits. Look, for example, at Fig. 19. Here the innermost curves of saddle-nodes of periodic orbits below the Hopf bifurcation line are approximations to the position of homoclinic tangencies. But clearly close to the Hopf line, the homoclinic tangency locus must be locally quadratic and cannot cross the Hopf line as the curves of saddle-nodes do. We conclude that this method of computing curves of homoclinic tangencies, is not accurate near Shil'nikov-Hopf bifurcation points. A method more likely to achieve accurate results is a direct approach; computing the periodic orbit and solutions in its stable and unstable manifolds. The implementation of such a method is left for future work, but see for example Beyn (1994) and Champneys & Lord (1997) for some indications.

Clearly we have not attempted to explain the complete dynamics in a neighbourhood of a non-transverse Shil'nikov-Hopf bifurcation. We have not mentioned at all the behaviour of strange attractors, or of secondary bifurcations of periodic orbits. In fact, for the example system, numerical experiments in the parameter range in question (with $\gamma \approx 0.4$) have shown that the shift dynamics associated with the homoclinic orbits and tangencies all lead to unstable chaotic invariant sets. However, preliminary results to be written up later show that to stabilise them it is necessary to put $c_3 > 0$.

Nor have we mentioned the connection between subsidiary homoclinic orbits and tangencies, as described in detail for the regular (codim 2) Shil'nikov-Hopf bifurcation by Hirschberg & Knobloch (1993). Instead we have attempted to explain a process by which loci of homoclinic orbits and homoclinic tangencies can become disconnected and to show that this naturally leads to isolas of periodic orbits in the parameter regimes of both homoclinic orbits *and* homoclinic tangencies. In fact, the analysis in either parameter regime could be taken independently of the nearby existence of the codim 3 point, indicating that isolas occur near non-transverse Shil'nikov homoclinic orbits or homoclinic tangencies to periodic orbits.

Finally, with reference to Fig. 11(a), we mention another possible codim 3 scenario that may cause the disconnection between Shil'nikov homoclinic orbits and homoclinic tangencies. An early conjecture on what happened to the locus of homoclinic orbits originating at the TB point as γ is decreased was that it collided with the point at which the Hopf bifurcation locus changes from being super to subcritical. (We now know that this is not the case, as shown by Figs. 11(c) and (d) and the accurate location of the non-transverse Shil'nikov-Hopf point.) Note from the unfolding of such a degenerate Hopf bifurcation (called a Bautin bifurcation in Kuznetsov (1995, Sect. 8.3)) that homoclinic orbits can only reach such a degenerate point in the case where the saddle-node of periodic orbits occurs on the side of where the equilibrium is completely unstable. In that case, after the Hopf bifurcation has become subcritical, the branch of homoclinic orbits would end in a 'blue sky catastrophe' when it hit the saddle-node of periodic orbits. A more complete analysis of this situation is left for future work.

Acknowledgements

ARC is extremely grateful to the *Consejería de Educación y Ciencia de la Junta de Andalucía* for financial support during a visit to Seville. We also thank Carlo Laing and a referee for their helpful comments on an earlier draft.

References

Algaba, A., Freire, E., Gamero, E. & Rodríguez-Luis, A. J. (1998), 'Analysis of Hopf and Takens-

Bogdanov bifurcations in a modified van der Pol-Duffing oscillator', *Nonlinear Dynamics* **16**, 369–404.

Belyakov, L. A. (1974), 'A case of the generation of a periodic motion with homoclinic curves', *Mat. Zam.* **15**, 336–341.

Beyn, W. J. (1994), On well-posed problems for connecting orbits in dynamical systems, *in* P. Kloeden & K. Palmer, eds, 'Proceedings of 'Chaotic Numerics', Geelong 1993'.

Bosch, M. & Simó, C. (1993), 'Attractors in a Shil'nikov–Hopf scenario and a related one-dimensional map', *Physica D* **62**, 217–229.

Bykov, V. V. (1993), 'The bifurcations of separatrix contours and chaos', *Physica D* **62**, 290–299.

Champneys, A. R. (1991), 'Homoclinic orbits in the dynamics of articulated pipes conveying fluid', *Nonlinearity* **4**, 747–774.

Champneys, A. R. & Kuznetsov, Y. A. (1994), 'Numerical detection and continuation of codimension-two homoclinic bifurcations', *Int. J. Bifurcation and Chaos* **4**, 795–822.

Champneys, A. R. & Lord, G. J. (1997), 'Computation of homoclinic solutions to periodic orbits in a reduced water-wave problem', *Physica D* **102**, 101–124.

Champneys, A. R., Kuznetsov, Y. & Sandstede, B. (1996), 'A numerical toolbox for homoclinic bifurcation analysis', *Int. J. Bifurcation and Chaos* **6**, 867–887.

Deng, B. & Sakamoto, K. (1995), 'Šil'nikov-Hopf bifurcations', *J. Diff. Eqns.* **119**, 1–23.

Doedel, E. J., Champneys, A. R., Fairgrieve, T. F., Kuznetsov, Y. A., Sandstede, B. & Wang, X. (1997), 'AUTO97 Continuation and bifurcation software for ordinary differential equations'. Available by anonymous ftp from `ftp.cs.concordia.ca` directory `pub/doedel/auto`.

Doedel, E., Keller, H. B. & Kernévez, J. P. (1991), 'Numerical analysis and control of bifurcation problems', *Int. J. Bifurcation and Chaos* **1**, 493–520, 745–772.

Fernández-Sánchez, F., Freire, E. & Rodríguez-Luis, A. J. (1997*a*), T-points in a Z_2 electronic oscillator. (I) analysis, Preprint, University of Seville.

Fernández-Sánchez, F., Freire, E. & Rodríguez-Luis, A. J. (1997*b*), 'Isolas, cusps and global bifurcations in an electronic oscillator', *Dynamics and Stability of Systems* **12**, 319–336.

Fernández-Sánchez, F., Freire, E., Gamero, E. & Rodríguez-Luis, A. J. (1997), T-points in a Z_2 electronic oscillator. (II) trip between a triple-zero and a Hopf bifurcation, Preprint, University of Seville.

Freire, E., Rodríguez-Luis, A. J., Gamero, E. & Ponce, E. (1993), 'A case study for homoclinic chaos in an autonomous electronic circuit. A trip from Takens–Bogdanov to Hopf–Shil'nikov', *Physica D* **62**, 230–253.

Gamero, E., Freire, E., Rodríguez-Luis, A. J., Ponce, E. & Algaba, A. (1993), Hypernormal form calculation for triple zero degeneracy, To appear in *Bulletin de la Societé Mathematique de Belgique, Serie A*.

Gaspard, P. (1987), Tangences Homoclines dans les Systèmes Dynamiques Dissipatifs, PhD thesis, Université Libre de Bruxelles.

Gaspard, P. & Wang, X.-J. (1987), 'Homoclinic orbits and mixed-mode oscillations in far-from-equilibrium systems', *J. Stat. Phys.* **48**, 151–199.

Gavrilov, N. K. & Shil'nikov, L. P. (1972), 'On three-dimensional systems close to systems with a structurally unstable homoclinic curve: I', *Mat.* USSR *Sb.* **17**, 467–485.

Gavrilov, N. K. & Shil'nikov, L. P. (1973), 'On three-dimensional systems close to systems with a structurally unstable homoclinic curve: II', *Mat.* USSR *Sb.* **19**, 139–156.

Glendinning, P. (1984), 'Bifurcations near homoclinic orbits with symmetry', *Phys. Lett. A* **103**, 163–166.

Glendinning, P. & Sparrow, C. T. (1984), 'Local and global behaviour near homoclinic orbits', *J. Stat. Phys.* **35**, 645–696.

Glendinning, P. & Sparrow, C. T. (1986), 'T-points: A codimension two heteroclinic bifurcation', *J. Stat. Phys.* **43**, 479–488.

Golubitsky, M. & Schaeffer, D. G. (1985), *Singularities and Groups in Bifurcation Theory, Volume I*, Applied Mathematical Sciences 51, Springer-Verlag, Berlin.

Guckenheimer, J. & Holmes, P. (1983), *Nonlinear Oscillations, Dynamical Systems and Bifurcations of Vector Fields*, Springer-Verlag, New York.

Hirschberg, P. & Knobloch, E. (1993), 'Šil'nikov–Hopf bifurcation', *Physica D* **62**, 202–216.

Hirschberg, P. & Laing, C. (1995), 'Sucessive homoclinic tangencies to a limit cycle', *Physica D* **89**, 1–14.

Kuznetsov, Y. A. (1995), *Elements of Applied Bifurcation Theory*, Applied Mathematical Sciences 112, Springer-Verlag, Berlin.

Lin, X.-B. (1993), Homoclinic bifurcations with weakly-expanding center manifolds, To appear in *Dynamics Reported*.

Newhouse, S. (1979), 'The abundance of wild hyperbolic sets and non-smooth stable sets', *Publ. I.H.E.S.* **50**, 101–151.

Sandstede, B. (1993), Verzweigungstheorie homokliner Verdopplungen, PhD thesis, Institut fur Angewandte Analysis und Stochastik, Berlin.

Shil'nikov, L. P. (1970), 'A contribution to the problem of the structure of an extended neighborhood of a rough equilibrium state of saddle-focus type', *Mat.* USSR *Sb.* **10**, 91–102.

Wiggins, S. (1990), *Introduction to Applied Nonlinear Dynamical Systems and Chaos*, Springer-Verlag, New York.